A Designed Photoenzyme for Enantioselective [2+2]-Cycloadditions

DOI:
10.1038/s41586-022-05335-3

Document Version
Accepted author manuscript

A Designed Photoenzyme for Enantioselective [2+2]-Cycloadditions

Jonathan S. Trimble,[1†] Rebecca Crawshaw,[1†] Florence J. Hardy,[1] Colin W. Levy,[1] Murray J.B. Brown,[2] Douglas E. Fuerst,[3] Derren J. Heyes,[1] Richard Obexer,[1] Anthony P. Green[1*]

[*] - Corresponding author
[†] - these authors contributed equally
[1]Department of Chemistry & Manchester Institute of Biotechnology, The University of Manchester, 131 Princess Street, Manchester, M1 7DN, U.K.
[2]Synthetic Biochemistry, Medicine Development and Supply, GlaxoSmithKline Medicines Research Centre, Stevenage, SG1 2NY, U.K.
[3]Synthetic Biochemistry, Medicine Development and Supply, GlaxoSmithKline, Collegeville, PA, U.S.A.

Abstract

The ability to programme new modes of catalysis into proteins would allow the development of enzyme families with functions beyond those found in nature. To this end, genetic code expansion methodology holds particular promise, as it allows the site-selective introduction of new functional elements into proteins as non-canonical amino acid side chains.[1-4] Here, we exploit an expanded genetic code to develop a photoenzyme that operates *via* triplet energy transfer catalysis, a versatile mode of reactivity in organic synthesis that is currently not accessible to biocatalysis.[5-12] Installation of a genetically encoded photosensitiser into the beta-propeller scaffold of DA_20_00[13] converts a *de novo* Diels-Alderase into a photoenzyme for [2+2]-cycloadditions (EnT1.0). Subsequent development and implementation of a platform for photoenzyme evolution afforded an efficient and enantioselective enzyme (EnT1.3, up to 99% *e.e.*) that can promote intramolecular and bimolecular cycloadditions, including transformations that have proven challenging to achieve selectively with small molecule catalysts. EnT1.3 performs >300 turnovers and, in contrast to small molecule photocatalysts, can operate effectively under aerobic conditions and at ambient temperatures. An X-ray crystal structure of an EnT1.3-product complex shows how multiple functional components work in synergy to promote efficient and selective photocatalysis. This study opens up a wealth of new excited-state chemistry in protein active sites and establishes the framework for developing a new generation of enantioselective photocatalysts.

Triplet energy transfer (EnT) photocatalysis promotes a broad range of valuable chemical transformations including cycloadditions, electrocyclic reactions, deracemizations, migrations, and rearrangements, many of which are not accessible from the ground state.[5-12] Photons offer a convenient and tuneable source of energy to selectively access reactive excited state intermediates under mild reaction conditions. Perhaps the most prominent class of photochemical reactions are [2+2]-cycloadditions, which construct cyclobutanes, oxetanes and azetidines.[14-16] In contrast to the analogous Diels-Alder [4+2]-cycloadditions, [2+2]-cycloadditions are thermally forbidden due to incompatible ground state orbital symmetries (Figure 1A). The key stages of EnT photocatalysis are shown in Figure 1B. Light energy is used to promote a triplet sensitiser from the ground state (S_0) to a singlet excited state (S_1), which then undergoes intersystem crossing to a triplet state (T_1). Since relaxation from T_1 to S_0 is spin-forbidden, triplet intermediates are relatively long-lived compared with singlet excited states. Commonly employed triplet photosensitisers include conjugated aromatic ketones such as benzophenone, xanthone, and thioxanthone, which display high quantum efficiencies for population of

the triplet state. The next step involves energy transfer from the triplet photosensitiser to the substrate in an overall spin-allowed process that returns the photosensitiser to the S_0 level and simultaneously promotes the substrate from S_0 to the reactive T_1 state, which can then undergo a variety of intra- and intermolecular processes.[5,6]

Enantioselective versions of photochemical reactions have been developed through dual catalytic strategies that combine an achiral photosensitiser with a photochemically inactive chiral catalyst (Figure 1C),[17-19] or by employing chiral photosensitisers (Figure 1D).[15,20] Although powerful, these approaches do not offer a general solution, and many desirable photochemical processes are not amenable to enantioselective catalysis. Furthermore, these reactions are oxygen sensitive, often require high catalyst loadings, and are restricted to a narrow range of substrates, with even small structural changes leading to substantial reductions in activity or selectivity.[21] In principle, enzyme active sites could offer more versatile chiral environments for mediating enantioselective photochemistry, where multiple functional elements can be accurately positioned within a single pocket. Through directed evolution these active sites could be sculpted to maximise productive interactions between the protein, substrate and photosensitiser to deliver efficient and selective photocatalysts (Figure 1E). However, while a handful of natural photoenzymes and engineered biocatalysts have been reported,[22-34] enzymes that mediate enantioselective EnT processes are currently unknown.

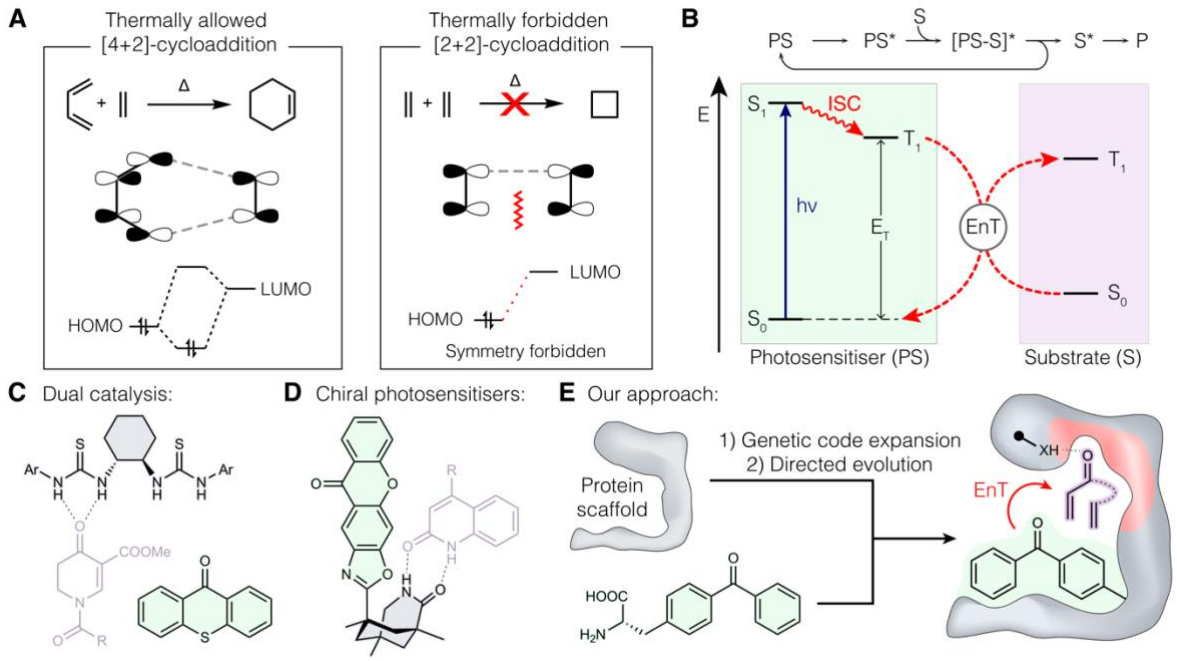

Figure 1. Photochemistry of [2+2]-cycloadditions. A. Comparison of thermally allowed [4+2]- and thermally forbidden [2+2]-cycloadditions and their ground state orbital interactions. **B.** Jablonski diagram representation of EnT photocatalysis. A photosensitiser (PS) is excited into a singlet state (S_1), which subsequently undergoes intersystem crossing (ISC) to the triplet state (T_1). EnT returns the PS to ground state, while exciting the substrate into T_1. **C-D.** Enantioselective EnT photocatalysis can be achieved using achiral photosensitisers in combination with chiral co-catalysts[18,19] or using chiral photosensitisers.[20] **E.** The approach to photoenzyme development described in this manuscript, involving selective installation of a genetically encoded photosensitiser into a protein scaffold and subsequent optimisation of the modified protein by directed evolution.

Photoenzyme design and evolution

To develop a selective photoenzyme, we chose the computationally designed Diels-Alderase DA_20_00 as a host scaffold.[13] The DA_20_00 active site contains designed hydrogen bonding residues (Tyr121 and Gln195) intended to promote the Diels-Alder reaction, which may prove useful in supporting catalysis of [2+2]-cycloadditions. These residues are embedded within a large hydrophobic pocket suitable for accommodating a bulky aromatic photosensitiser (Figure 2A). To unlock photocatalytic activity, an engineered *Methanococcus jannaschii* tyrosyl-tRNAsynthetase/tyrosyl-tRNA (*Mj*TyrRS/*Mj*tRNA^{Tyr}) pair was used to incorporate 4-benzoylphenylalanine (BpA) at several positions around the DA_20_00 active site pocket (Extended Data Figure 1).[35] Intramolecular [2+2]-cycloaddition of quinolone **1** was selected as the target transformation (Figure 2B).[20] Benzophenone (BP) is a suitable photosensitiser for this reaction and gives rise to racemic straight and crossed chain products (**1a** and **1b**) as a 1.4:1 mixture of regioisomers (Figure 2C). Placement of BpA at position 173 within the hydrophobic pocket of DA_20_00 provided the active photoenzyme EnT1.0, which is a more effective catalyst than BP and displays modest levels of regio- (2:1, **1a**:**1b**) and enantioselectivity (46% *e.e.* for the major product (-)-**1a**). EnT1.0 activity is strictly dependent on light and the presence of the BpA173 photosensitiser (Figure 2C).

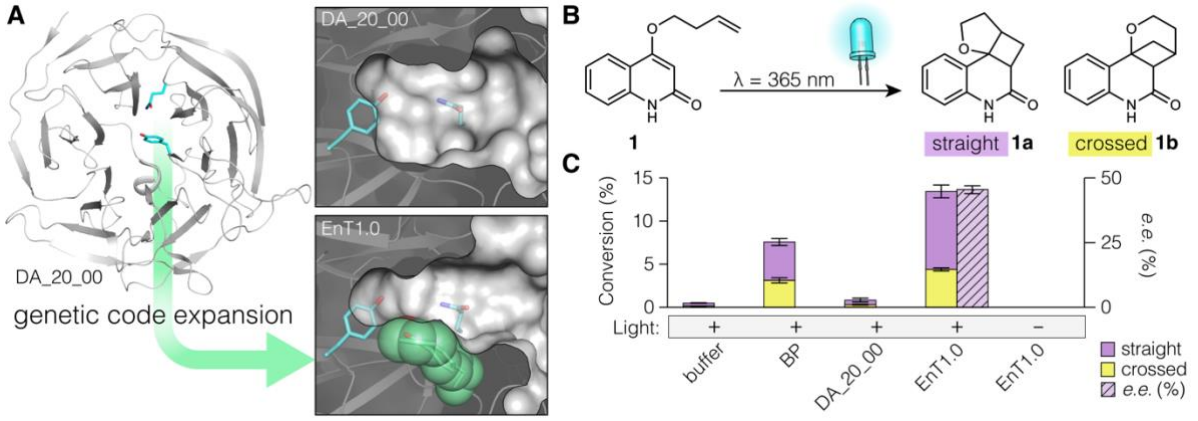

Figure 2. Development of the first-generation photoenzyme, EnT1.0. A. Genetic incorporation of a BpA photosensitiser (green CPK spheres) into the hydrophobic core of DA_20_00 (PDB: 3I1C) afforded the first-generation photocatalyst EnT1.0 (PDB: 7ZP5). **B.** Intramolecular [2+2]-photocycloaddition of 4-(but-3-en-1-yloxy)quinolin-2(1H)-one (**1**) gives rise to two regioisomeric products, 3,3a,4,4a-tetrahydro-2H-furo[2',3':2,3]cyclobuta[1,2-c]quinolin-5(6H)-one (**1a**) and 2,3,4,4a-tetrahydro-4,10b-methanopyrano[3,2-c]quinolin-5(6H)-one (**1b**) **C.** Bar chart showing the conversion of **1** to **1a** and **1b** by EnT1.0, BP, and the unmodified protein DA_20_00. Reaction conditions: 15 μM catalyst (BP or protein variant), 400 μM **1**, 30 minutes irradiation at 365 nm, 4 °C. EnT1.0 activity is dependent on light and affords the major product (-)-**1a** with 46% *e.e.*. Conversion and selectivity data are given in Supplementary Table 1. Error bars represent the standard deviation of measurements made in triplicate.

To improve EnT1.0 activity, we initially mutated eight residues that lie in proximity to BpA173 to alanine (Extended Data Figure 2). An M90A mutation gave rise to a substantial 3-fold increase in conversion to **1a** along with a modest improvement in enantioselectivity to 60% *e.e.* (EnT1.1, Figure 3, Extended Data Figure 2). This improved variant facilitated detection of enzyme activity in clarified cell lysate, and enabled the development of a directed evolution workflow suitable for high-throughput engineering of triplet energy transfer photoenzymes. This evolutionary workflow relies on uniform irradiation of enzyme variants arrayed in microtiter plates, which was achieved using a commercial

LED array (see Experimental Procedures). The observed coefficient of variance across an assay plate using purified EnT1.0 was shown to be less than 5% (Supplementary Figure 1), a value that is in line with established high-throughput screening methods.

The evolutionary strategy consisted of two rounds of saturation mutagenesis targeting residues in the active site and second coordination sphere, which were individually randomised using NNK degenerate codons. Individual variants arrayed in 96-well microtiter plates were irradiated for 30 mins at 365nm using an LED array in the presence of substrate **1** and reactions analysed by high-throughput ultra-performance liquid chromatography (UPLC, Supplementary Figure 2-3). The most active (~1%) clones, identified based on conversion to **1a**, were then evaluated as purified proteins for improved activity and enantioselectivity (Supplementary Figure 4). Beneficial mutations identified during each round were subsequently combined by DNA shuffling. Following evaluation of ~3500 library members, an EnT1.3 variant emerged with improved activity, stability, and selectivity. EnT1.3 contains five mutations (EnT1.0 M90A Q149D P196R K225E A229S, Extended Data Figure 3) and achieves a substantial 10-fold improvement in reaction conversion of **1** to **1a** compared with EnT1.0 following 30 minutes of irradiation (Figure 3C & 3D). The enhanced performance of EnT1.3 arises from a combination of a 4-fold increase in initial rate (Extended Data Figure 4), improved regioselectivity (**1a**:**1b** 2:1 for EnT1.0 vs 9:1 for EnT1.3, Figure 3C), and reduced susceptibility to photo-deactivation, that likely arises in EnT1.0 from an intramolecular photo-crosslinking process involving the benzophenone side chain (Extended Data Figure 5). EnT1.3 also offers high levels of enantio-control, generating (-)-**1a** with >99% *e.e.*. Interestingly, EnT1.3 is more active at 4 °C than at room temperature (Extended Data Figure 6), which may reflect an increased lifetime of the photosensitiser triplet state at lower temperatures.[36] To gain insight into the kinetic parameters of EnT1.3, we determined initial reaction velocities across a range of substrate concentrations (Supplementary Figure 7A). These measurements reveal that EnT1.3 has a high affinity for **1** (K_M < 40 μM), which precludes accurate determination of K_M due to the detection limits of HPLC analysis. A k_{cat} of 1.3 +/- 0.04 min^{-1} was determined under the assay conditions used throughout enzyme engineering, although this value is linearly dependent on light intensity and so can be increased at higher powers (Supplementary Figure 7B).

In contrast to small-molecule photocatalysts, which are highly sensitive to oxygen due to triplet quenching, EnT1.3 is tolerant of aerobic buffers (Figure 3D) and can achieve >300 turnovers under these conditions (Extended Data Figure 7). Presumably the EnT1.3 active site excludes oxygen to minimize triplet quenching and favour productive energy transfer to substrate. In line with these observations, laser pulse experiments reveal that the triplet lifetime of the enzyme-bound BpA chromophore is very similar in aerobic and anaerobic buffers, which contrasts with the oxygen sensitivity of triplet benzophenone in solution (Supplementary Figure 8). With only 1.5 mol% EnT1.3, near complete conversion of **1** to optically pure (-)-**1a** can be achieved within 2 hr (Supplementary Table 3), underscoring the efficiency of our engineered photoenzyme. Compared to small chiral photocatalysts, EnT1.3 achieves higher conversion, regioselectivity and enantioselectivity using lower catalyst loadings.[20] The enzyme also operates efficiently at ambient temperatures compared with the cryogenic temperatures needed with small chiral catalysts. To demonstrate practical utility, we performed a preparative scale biotransformation to afford enantiopure (-)-**1a**, along with its minor regioisomer **1b**, as the sole products in essentially quantitative (95%) yield (Supplementary Figure 9).

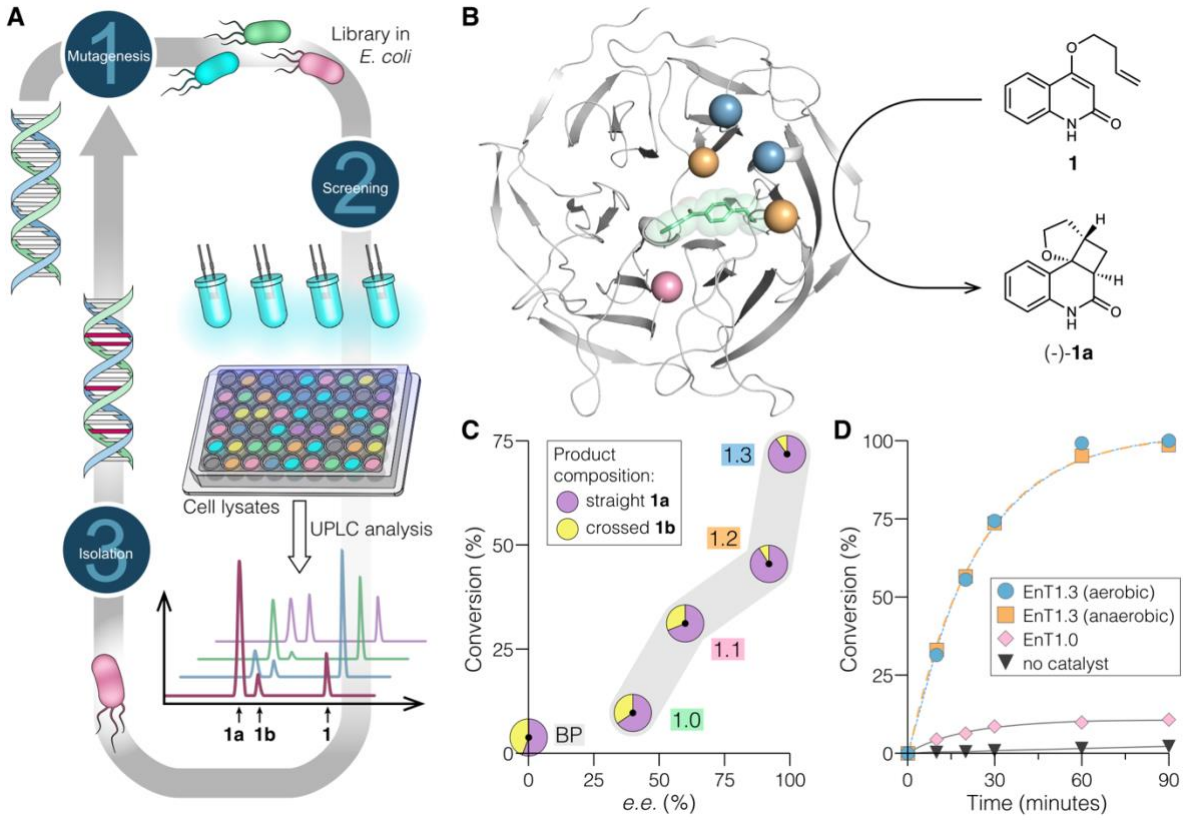

Figure 3: Directed evolution of an efficient and enantioselective photoenzyme. A. Schematic of the directed evolution workflow for photoenzyme engineering. **B.** Mutational map of EnT1.3, highlighting the encoded photosensitiser BpA173 (green sticks and semi-transparent CPK spheres) and residues installed during alanine scanning (pink sphere) and rounds 1 and 2 of evolution (peach and blue spheres, respectively). **C.** Reaction conversion, regioselectivity, and enantioselectivity were improved along the evolutionary trajectory. Reaction conditions: 10 µM (2.5 mol%) catalyst (BP or protein variant), 400 µM **1**, 30 minutes irradiation at 365 nm, 4 °C. The ratio of **1a**:**1b** is represented as a pie chart and *e.e.* is given for (-)-**1a**. All conversion and selectivity data, including standard deviations, are given in Extended Data Figure 8. **D.** Reaction time-courses (**1** to **1a** and **1b,** 10 µM (2.5 mol%) catalyst, 400 µM **1**, 365 nm, 4 °C) catalysed by EnT1.0 (pink) and EnT1.3 (blue). A comparison of EnT1.3 activity under anaerobic conditions is shown in orange.

EnT1.3 is a versatile [2+2]-cyclase

We next explored the photocatalytic activity of EnT1.3 towards [2+2]-cycloadditions of allyloxy-, alken-1-yl-, and allyloxy(methyl)- quinolones to generate optically enriched products (**2a-13a**, Figure 4). High conversions and selectivities were achieved in the majority of cases. With substrates **3**, **8** and **12**, introduction of a gem-dimethyl moiety led to a reduction in enantioselectivity likely due to a high degree of shape-complementarity between the EnT1.3 active site and substrate **1** (*vide infra*). Consistent with this interpretation, the less highly evolved EnT1.2 variant gave improved activity and selectivity with **3** and **12**, while EnT1.1 A229S Y37L was found to be a superior variant for conversion of substrate **8**. The ability of EnT1.3 to generate **2a** and **7a** with high levels of stereocontrol is particularly noteworthy. Analogous reactions with small chiral photosensitisers proceed with poor selectivity, as cyclizations to form 6-membered ring analogues are relatively slow and competing dissociation of the excited substrate from the photosensitiser erodes *e.e.*.[5,15,21] These examples show that our enzymes can mediate selective transformations even when downstream excited state chemistry is normally slow.

Small molecule chiral photosensitisers also rely on complementary dual hydrogen-bonding contacts between the substrate and catalyst to achieve enantioselective photochemistry.[20] To demonstrate that protein catalysts are not constrained in the same manner, we next investigated cycloaddition of an *N*-methyl derivative **13**. EnT1.3 affords optically enriched **13a**, along with its regioisomer **13b**, with modest selectivity (2:1 r.r., 36% *e.e.* for **13a**), which could be further enhanced by first introducing a rational Y121F mutation (4:1 r.r., 78% *e.e.* for **13a**) followed by a S271C substitution (8:1 r.r., 98% *e.e.* for **13a**) identified through subsequent directed evolution. This additional engineering demonstrates how protein active sites can be readily adapted to augment catalytic function and shows that our photoenzymes can mediate selective transformations of substrate classes that are beyond the reach of existing small-molecule systems. Finally, to expand synthetic utility, we explored the application of EnT1.3 towards bimolecular [2+2]-cycloadditions of 2-quinolone. Despite being optimised for an intramolecular reaction, EnT1.3 shows remarkable selectivity in bimolecular processes using methyl vinyl ketone or ethyl vinyl ketone as co-substrates, achieving 97% *e.e.* in both cases (Figure 4). Taken together, these studies highlight EnT1.3 and its variants as a versatile and powerful platform for the enantioselective construction of cyclobutane rings.

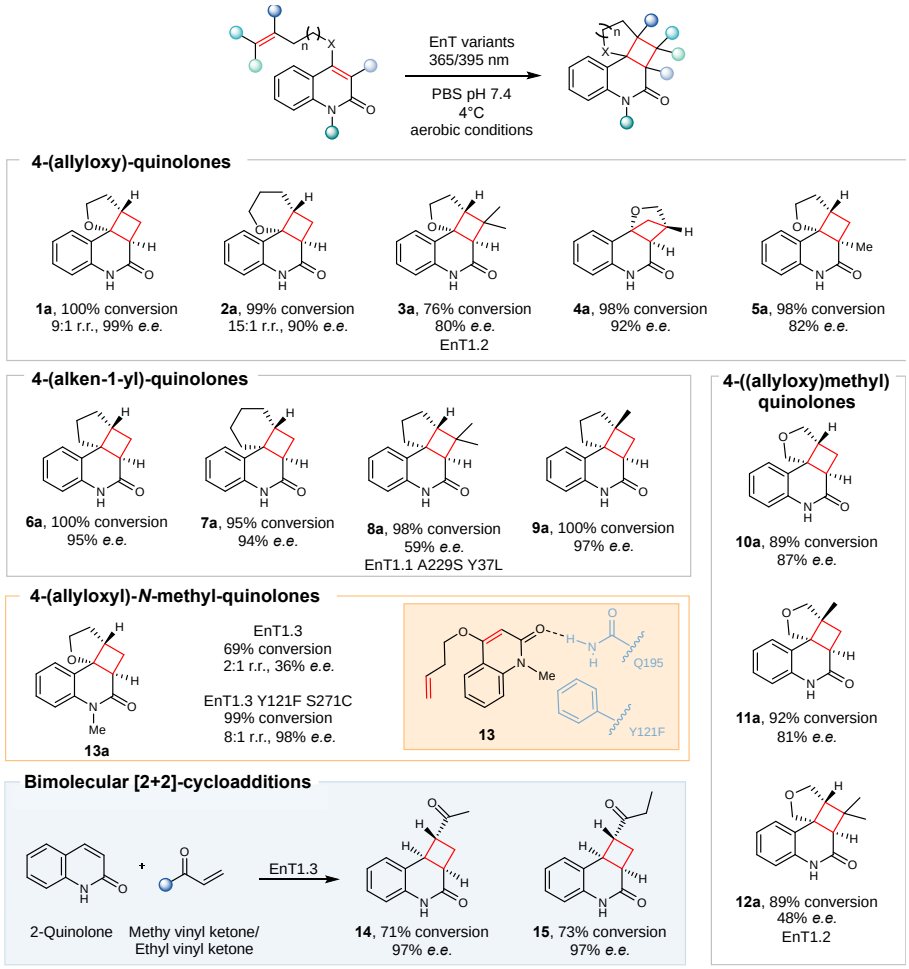

Figure 4: Substrate scope of EnT1.3 and selected variants. EnT1.3 promotes intramolecular [2+2]-cycloadditions on a range of quinolones to produce 4-(allyloxy)-, 4-(alken-1-yl)- and 4-((allyloxy)methyl)-quinolone derivatives **1a-2a**, **4a-7a**, and **9a-11a** with high conversions and selectivities. With substrates **3** and **12** EnT1.2 gave higher levels of activity and selectivity, while EnT1.1 A229S Y37L proved to be a superior variant for conversion of substrate **8**. With *N*-methyl quinolone **13**, reactions with EnT1.3 proceed with modest selectivity, which can be improved with a rational Y121F mutation and subsequent engineering to produce variant EnT1.3 Y121F S271C. EnT1.3

also promotes bimolecular cycloadditions of 2-quinolone with methyl vinyl ketone or ethyl vinyl ketone to produce **14** and **15**, respectively. Reaction conversions are the mean of biotransformations performed in triplicate. The absolute stereochemistry of products **2a**-**13a** were assigned by analogy to the product (-)-**1a**, formed by EnT1.3. The absolute stereochemistry of **14** was assigned by comparison of HPLC retention times following a literature procedure.[37] The absolute stereochemistry of **15** was assigned by analogy to the product **14**. Reaction conditions for the synthesis of **1a**–**15** are presented in Supplementary Table 3.

Structural basis for efficient catalysis

To gain insights into the EnT1.3 catalytic mechanism, a crystal structure of a C-terminally truncated analogue (EnT1.3$\Delta C_{310\text{-}314}$, see Supplementary Information) complexed with product (-)-**1a** was solved (1.7 Å, Figure 5, Supplementary Table 5). This truncation has negligible effect on catalytic activity or selectivity (Supplementary Figure 5), and was introduced to circumvent the C-terminus of a neighbouring chain from occluding the EnT1.3 active site *in crystallo*. The ligand sits in a snug active site pocket with its aromatic ring sandwiched between His287 and the benzophenone sidechain (3.6 Å and 3.8 Å respectively, Figure 5, Supplementary Figure 6). This pose presumably allows for efficient triplet energy transfer from the excited-state photosensitiser to the parent substrate. The well-packed active site led us to consider whether a non-covalent benzophenone sensitizer could support enantioselective catalysis in the EnT1.3 scaffold. However, reactions with EnT1.3 BpA173Ala in the presence of exogenous benzophenone led to low conversion and selectivity (Supplementary Table 3), highlighting the importance of installing the triplet photosensitizer on the genetic level. The crystal structure suggests that Trp244 may play a role in controlling reaction selectivity in favour of the formation of (-)-**1a** by shaping the active site cavity to prevent addition of the exocyclic alkene to the enantiotopic face of the excited quinolone. Indeed, a W244A mutation leads to a substantial reduction in activity and racemic product formation (Extended Data Figure 9). Ligand binding is further supported by complementary hydrogen bonding interactions with Tyr121, which serves as a hydrogen bond acceptor to the quinolone N-H, and Gln195, which acts as a hydrogen bond donor to the quinolone carbonyl (Figure 5). Interestingly, Tyr121 and Gln195 were designed to mediate Diels-Alder catalysis in DA_20_00 through hydrogen bonding interactions, albeit with opposite donor/acceptor relationships to those observed in EnT1.3. With substrate **1**, mutation of Tyr121 to Phe leads to a 3-fold reduction in activity along with a modest decrease in enantioselectivity (67% *e.e.*, Extended Data Figure 9). In contrast, this mutation improves both activity and selectivity towards *N*-methylated substrate **13** (Figure 4), where the *N*-methyl substituent likely occupies the position vacated by removal of the Tyr121 phenolic oxygen. The hydrogen bond from Gln195 to the quinolone carbonyl is particularly short (2.6 Å) and likely serves to lower the triplet energy of the substrate.[38] Mutation of Gln195 to Ala leads to a considerable reduction in activity and selectivity, underscoring its importance to EnT1.3 catalysis. Gln195 is anchored in position by an additional hydrogen bond with Arg196, which emerged during evolution. Interestingly, in apo-EnT1.3 Gln195 and Arg196 lie in markedly different orientations, with Arg196 instead interacting with Asp149 and Glu225, suggesting that substrate binding may induce formation of a productive Arg196-Gln195-substrate hydrogen bonding network (Extended Data Figure 10). This combined structural analysis offers a first glimpse into active site features governing efficient energy transfer catalysis, and provides an important blueprint for the future design of photoenzymes with new and augmented functions.

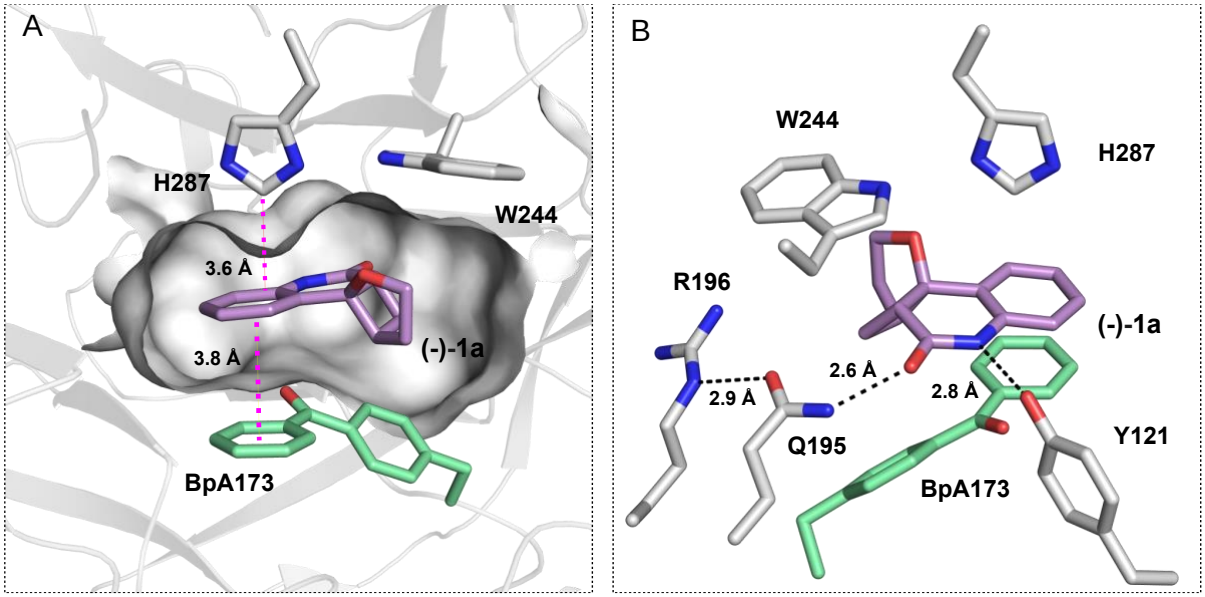

Figure 5: A 1.7 Å crystal structure of EnT1.3ΔC$_{310\text{-}314}$ in complex with product (-)-1a. A. The product (atom-coloured sticks, carbon purple) is well accommodated within the active site pocket (shown as a grey surface) in proximity to the BpA173 sidechain (atom-coloured sticks with green carbon), His287 and Trp244 (atom-coloured sticks, with grey carbon). π–stacking interactions are shown as pink dashed lines. **B.** Expanded view of the active site showing hydrogen bonding interactions (black dashed lines) involving R196, Q195, Y121 and the ligand.

Conclusion

In summary, our study provides a powerful demonstration of how an expanded genetic code can be used to embed entirely new modes of catalysis into proteins. This technology has allowed the development of a proficient photoenzyme that operates *via* a triplet energy transfer mechanism, a versatile reaction manifold in organic synthesis that was previously inaccessible to biocatalysis. While EnT1.3 was tailored to promote intramolecular [2+2]-cycloadditions, we anticipate that our approach can be readily adapted to alternative chemistries that are enabled by triplet energy transfer. In this regard, it is encouraging that EnT1.3 is able to mediate bimolecular processes and can be readily adapted to operate on substrates that are beyond the scope of small chiral photocatalysts. The catalytic performance and structural sophistication of EnT1.3 is particularly notable, given that <1000 protein variants were evaluated across the evolutionary trajectory. Presumably, more efficient photocatalysts will be generated through a deeper exploration of protein sequence. Likewise, combinations of high-throughput experimentation and *in silico* design will deliver active sites with new geometries and arrangements of functional groups suitable for mediating selective photocatalysis.[39] Thus with the mechanistic framework for embedding EnT catalysis into proteins now established, we are optimistic about the prospect of developing photoenzymes for a broad array of valuable photochemical processes.

References

1. Burke, A. J. *et al.* Design and evolution of an enzyme with a non-canonical organocatalytic mechanism. *Nature* **570**, 219–223 (2019).

2. Drienovská, I., Mayer, C., Dulson, C. & Roelfes, G. A designer enzyme for hydrazone and oxime formation featuring an unnatural catalytic aniline residue. *Nat. Chem.* **10**, 946–952 (2018).

3. Chin, J. W. Expanding and reprogramming the genetic code. *Nature* **550**, 53–60 (2017).

4. Liu, C. C. & Schultz, P. G. Adding New Chemistries to the Genetic Code. *Annu. Rev. Biochem.* **79**, 413–444 (2010).

5. Großkopf, J., Kratz, T., Rigotti, T. & Bach, T. Enantioselective Photochemical Reactions Enabled by Triplet Energy Transfer. *Chem. Rev.* **122**, 1626–1653 (2022).

6. Strieth-Kalthoff, F. & Glorius, F. Triplet Energy Transfer Photocatalysis: Unlocking the Next Level. *Chem* **6**, 1888–1903 (2020).

7. Tröster, A., Bauer, A., Jandl, C. & Bach, T. Enantioselective Visible-Light-Mediated Formation of 3-Cyclopropylquinolones by Triplet-Sensitized Deracemization. *Angew. Chem. Int. Ed.* **58**, 3538–3541 (2019).

8. Kleinmans, R. *et al.* Intermolecular [2π+2σ]-photocycloaddition enabled by triplet energy transfer. *Nature* (2022). doi:10.1038/s41586-022-04636-x

9. Alonso, R. & Bach, T. A Chiral Thioxanthone as an Organocatalyst for Enantioselective [2+2] Photocycloaddition Reactions Induced by Visible Light. *Angew. Chem. Int. Ed.* **53**, 4368–4371 (2014).

10. Münster, N., Parker, N. A., van Dijk, L., Paton, R. S. & Smith, M. D. Visible Light Photocatalysis of 6π Heterocyclization. *Angew. Chem. Int. Ed. Engl.* **56**, 9468–9472 (2017).

11. Huang, M., Zhang, L., Pan, T. & Luo, S. Deracemization through photochemical *E*/*Z* isomerization of enamines. *Science* **375**, 869–874 (2022).

12. Maturi, M. M., Pöthig, A. & Bach, T. Enantioselective Photochemical Rearrangements of Spirooxindole Epoxides Catalyzed by a Chiral Bifunctional Xanthone. *Aust. J. Chem.* **68**, 1682–1692 (2015).

13. Siegel, J. B. *et al.* Computational Design of an Enzyme Catalyst for a Stereoselective Bimolecular Diels-Alder Reaction. *Science* **329**, 309–313 (2010).

14. Becker, M. R., Richardson, A. D. & Schindler, C. S. Functionalized azetidines via visible light-enabled aza Paternò-Büchi reactions. *Nat. Commun.* **10**, 5095 (2019).

15. Müller, C. *et al.* Enantioselective Intramolecular [2 + 2]-Photocycloaddition Reactions of 4-Substituted Quinolones Catalyzed by a Chiral Sensitizer with a Hydrogen-Bonding Motif. *J. Am. Chem. Soc.* **133**, 16689–16697 (2011).

16. Vogt, F., Jödicke, K., Schröder, J. & Bach, T. Paternò–Büchi Reactions of Silyl Enol Ethers and Enamides. *Synthesis* **24**, 4268–4273 (2009).

17. Blum, T. R., Miller, Z. D., Bates, D. M., Guzei, I. A. & Yoon, T. P. Enantioselective photochemistry through Lewis acid catalyzed triplet energy transfer. *Science* **354**, 1391–1395 (2016).

18. Mayr, F., Brimioulle, R. & Bach, T. A Chiral Thiourea as a Template for Enantioselective Intramolecular [2 + 2] Photocycloaddition Reactions. *J. Org. Chem.* **81**, 6965–6971 (2016).

19. Hörman, F. M. *et al.* Triplet Energy Transfer from Ruthenium Complexes to Chiral

Eniminium Ions: Enantioselective Synthesis of Cyclobutanecarbaldehydes by [2+2] Photocycloaddition. *Angew. Chem. Int. Ed* **59**, 9659–9668 (2020).

20. Müller, C., Bauer, A. & Bach, T. Light-driven enantioselective organocatalysis. *Angew. Chem. Int. Ed. Engl.* **48**, 6640–6642 (2009).

21. Maturi, M. M. *et al.* Intramolecular [2+2] Photocycloaddition of 3- and 4-(But-3-enyl)oxyquinolones: Influence of the Alkene Substitution Pattern, Photophysical Studies, and Enantioselective Catalysis by a Chiral Sensitizer. *Chem. Eur. J.* **19**, 7461–7472 (2013).

22. Sorigué, D. *et al.* An algal photoenzyme converts fatty acids to hydrocarbons. *Science* **357**, 903–907 (2017).

23. Heyes, D. J. *et al.* Photochemical Mechanism of Light-Driven Fatty Acid Photodecarboxylase. *ACS Catal.* **10**, 6691–6696 (2020).

24. Heyes, D. J. *et al.* Photocatalysis as the 'master switch' of photomorphogenesis in early plant development. *Nat. Plants* **7**, 268–276 (2021).

25. Tan, C. *et al.* The molecular origin of high DNA-repair efficiency by photolyase. *Nat. Commun.* **6**, 7302 (2015).

26. Liu, X. *et al.* A genetically encoded photosensitizer protein facilitates the rational design of a miniature photocatalytic CO2-reducing enzyme. *Nat. Chem.* **10**, 1201–1206 (2018).

27. Black, M. J. *et al.* Asymmetric redox-neutral radical cyclization catalysed by flavin-dependent 'ene'-reductases. *Nat. Chem.* **12**, 71–75 (2020).

28. Gao, X., Turek-Herman, J. R., Choi, Y. J., Cohen, R. D. & Hyster, T. K. Photoenzymatic Synthesis of α-Tertiary Amines by Engineered Flavin-Dependent "Ene"-Reductases. *J. Am. Chem. Soc.* **143**, 19643–19647 (2021).

29. Emmanuel, M. A., Greenberg, N. R., Oblinsky, D. G. & Hyster, T. K. Accessing non-natural reactivity by irradiating nicotinamide-dependent enzymes with light. *Nature* **540**, 414–417 (2016).

30. Huang, X. *et al.* Photoinduced chemomimetic biocatalysis for enantioselective intermolecular radical conjugate addition. *Nat. Catal.* (2022). doi:10.1038/s41929-022-00777-4

31. Huang, X. *et al.* Photoenzymatic enantioselective intermolecular radical hydroalkylation. *Nature* **584**, 69–74 (2020).

32. Bulina, M. E. *et al.* A genetically encoded photosensitizer. *Nat. Biotechnol.* **24**, 95–99 (2006).

33. Fu, Y. *et al.* Biocatalytic Cross-Coupling of Aryl Halides with a Genetically Engineered Photosensitizer Artificial Dehalogenase. *J. Am. Chem. Soc.* **143**, 617–622 (2021).

34. Kang, F. *et al.* Rational Design of a Miniature Photocatalytic CO2-Reducing Enzyme. *ACS Catal.* **11**, 5628–5635 (2021).

35. Chin, J. W., Martin, A. B., King, D. S., Wang, L. & Schultz, P. G. Addition of a photocrosslinking amino acid to the genetic code of Escherichia coli. *Proc. Natl. Acad. Sci. U. S. A.* **99**, 11020–11024 (2002).

36. Godfrey, T. S., Hilpern, J. W. & Porter, G. Triplet-triplet absorption spectra of benzophenone and its derivatives. *Chem. Phys. Lett.* **1**, 490–492 (1967).

37. Tröster, A., Alonso, R., Bauer, A. & Bach, T. Enantioselective Intermolecular [2 + 2] Photocycloaddition Reactions of 2(1H)-Quinolones Induced by Visible Light Irradiation. *J. Am. Chem. Soc.* **138**, 7808–7811 (2016).

38. Daub, M. E. *et al.* Enantioselective [2+2] Cycloadditions of Cinnamate Esters: Generalizing

Lewis Acid Catalysis of Triplet Energy Transfer. *J. Am. Chem. Soc.* **141**, 9543–9547 (2019).

39. Lovelock, S. L. *et al.* The Road to Fully Programmable Protein Catalysis. *Nature* **606**, 49-58 (2022).

Data Availability Statement

Coordinates and structure factors have been deposited in the Protein Data Bank under accession numbers 7ZP5, 7ZP6 and 7ZP7. The authors declare that the data supporting the findings of this study are available within the paper and its Supplementary Information files. Source data are available from the corresponding author upon reasonable request.

Acknowledgements

We acknowledge the European Research Council (ERC Starter Grant no. 757991 to A.P.G.) and the Biotechnology and Biological Sciences Research Council (David Phillips Fellowship BB/M027023/1 to A.P.G. and Transition Award BB/W014483/1). J.S.T was supported by an integrated catalysis Doctoral Training Programme (EP/023755/1). R.C was supported by a BBSRC Flexible Talent Mobility Account Award (BB/S507969/1). We are grateful to the Diamond Light Source for time on beamline i03 under proposal MX24447, to the Manchester SYNBIOCHEM Centre (BB/M017702/1), the Future Biomanufacturing Hub (EP/S01778X/1) and the Henry Royce Institute for Advanced Materials (funded through EPSRC grants nos. EP/R00661X/1, EP/S019367/1, EP/P025021/1 and EP/P025498/1) for access to their facilities, and to M. Dunstan (Manchester Institute of Biotechnology) for guidance on automating directed evolution workflows. We thank R. Spiess and R. Sung (Manchester Institute of Biotechnology) for acquiring protein mass spectra and for assistance with UPLC method development, and Reach Separations (Nottingham) for supplying individual enantiomers of the product **1a**. We thank Sarah Lovelock and Romain Jamagne for their assistance in preparing DNA constructs and modified proteins. We are grateful to GlaxoSmithKline for access to their facilities, and to Joseph Hosford and Lee J. Edwards (GlaxoSmithKline, Stevenage) for helpful discussions. We are also grateful to Prof. Daniele Leonori for helpful discussions throughout the project.

Author Contributions

J.S.T carried out organic synthesis and substrate profiling of EnT variants. R.C. carried out molecular biology, directed evolution experiments and protein crystallisation. J.S.T and R.C carried out protein production, assay development and photochemical assays. F.J.H. and C.L. interpreted, analysed and presented structural data. R.O., D.H., M.J.B.B., and D.F. contributed to experimental design and data analysis. A.P.G, J.S.T, R.C. F.J.H, and R.O. discussed the results and participated in writing the manuscript. All authors provided input throughout project progression. A.P.G. initiated and directed the research.

Competing Interests

The authors declare no competing interests.

Additional Information

Supplementary Information is available for this paper. Correspondence and requests for materials should be addressed to anthony.green@manchester.ac.uk.

Methods

Materials:

All chemicals and biological materials were obtained from commercial suppliers. Lysozyme, DNase I, chloramphenicol and kanamycin were purchased from Sigma-Aldrich; polymyxin B sulfate from AlfaAesar; LB agar, LB media, 2xYT media, Isopropyl-β-d-1-thiogalactopyranoside (IPTG) and arabinose from Formedium; (S)-2-Amino-3-(4-benzoylphenyl)propanoic acid from Flurochem; the pEVOL_pBpA/tRNA$_{CUA}$ plasmid[32] was purchased from Addgene; *Escherichia coli* (*E. coli*) BL21(DE3), *Escherichia coli* (*E. coli*) 5α, Q5 DNA polymerase, T4 DNA ligase and restriction enzymes from New England BioLabs; and oligonucleotides and genes were synthesized by Integrated DNA Technologies.

Construction of pET-29b_EnT1.0 and variants:

The original DA_20_00 design[13] was subcloned using *NdeI* and *XhoI* restriction sites into a pET-29b(+) vector containing a C-terminal His$_6$-tag to yield pET-29b(+)_DA_20_00. The Ala173BpA mutation was introduced by replacing the Ala173 codon with a TAG stop codon using QuikChange site-directed mutagenesis (Agilent) to yield pET-29b(+)_EnT1.0. Point mutants of EnT1.0 and variants were constructed using the same procedure.

Protein production and purification:

For expression of EnT1.0 and its variants, chemically competent *E. coli* BL21(DE3) cells containing pEVOL_pBpA/tRNA$_{CUA}$[32] were transformed with the appropriate pET29b(+) construct. A single colony of freshly transformed cells was used to inoculate 5 mL LB medium containing 50 μg mL^{-1} kanamycin and 25 μg mL^{-1} chloramphenicol and cultured for 18h at 37 ˚C and 200 r.p.m.. Starter cultures (500 μL) were used to inoculate 50 ml 2xYT medium supplemented with 50 μg mL^{-1} kanamycin, 25 μg mL^{-1} chloramphenicol and 1 mM (S)-2-Amino-3-(4-benzoylphenyl)propanoic acid (BpA), which was added as a 1 M stock dissolved in 1 M NaOH. Cultures were grown at 37°C, 200 r.p.m. to an optical density at 600 nm (OD$_{600}$) of ~0.6 A.U.. Protein expression was induced with the addition of L-arabinose to a final concentration of 0.05% and IPTG to a final concentration of 0.1 mM. Induced cultures were incubated for 20 h at 25 °C and the cells were subsequently collected by centrifugation (3,220*g* for 10 min). Pelleted cells were resuspended in lysis buffer (50 mM HEPES, 300 mM NaCl, pH 7.5 containing 20 mM imidazole) and lysed by sonication (1 second on/off, 5 minutes total sonication) at 4 ˚C with the addition of 1 μg mL^{-1} DNase I. Cell lysates were clarified by centrifugation (27,216*g* for 30 min), and supernatants were subjected to affinity chromatography using Ni-NTA Agarose (Qiagen). His$_6$-tagged proteins were eluted using 50 mM HEPES, 300 mM NaCl, pH 7.5 containing 250 mM imidazole. Buffer exchange of purified proteins was performed using 10DG desalting columns (Bio-Rad) and PBS pH 7.4 (137 mM NaCl; 2.7 mM KCl; 10 mM Na_2HPO_4; 1.8 mM KH_2PO_4) and analysed by SDS–PAGE. Proteins were aliquoted, flash-frozen in liquid nitrogen, and stored at −80 °C. Protein concentrations were determined by NanoDrop™ using an extinction coefficient of 46,410 M^{-1} cm^{-1} for DA_20_00 and 62,152 M^{-1} cm^{-1} for EnT1.0 and variants. Extinction coefficients for variants containing BpA were deduced through a comparison of DA_20_00 and EnT1.0 using a BCA Protein Assay kit (Thermofisher).

Mass spectrometry:

Purified protein samples were desalted on 10k MWCO Vivaspin centrifugal concentrators (Sartorius) using 0.1% acetic acid and diluted to a final concentration of 0.4 mg mL^{-1}. Mass spectrometry was performed on a 1200 series Agilent LC in conjunction with a Agilent QTOF 6510. A 5 μL sample injection was performed followed by a 1 min 5% acetonitrile (with 0.1% formic acid) isocratic wash. Protein was eluted over 1 min using 95% acetonitrile with 5% water. The resulting multiply charged

spectrum was deconvoluted using Agilent MassHunter Software. Protein mass spectrometry results are displayed in Supplementary Information, Table S7.

Library construction:

Rounds 1,2 and 3: Saturation mutagenesis. Positions were individually randomised using degenerate NNK codons. DNA libraries were constructed by overlap extension PCR. Primers for library generation are given in Supplementary Information Table S11. Assembled genes and pET29b(+) vector were digested using *NdeI* and *XhoI* endonucleases, gel-purified and subsequently ligated using T4 DNA ligase in a 5:1 ratio, respectively. Ligations were transformed into *Escherichia coli* (*E. coli*) 5α cells, resulting colonies were pooled and plasmid DNA was extracted using a Mini-prep kit (Quiagen) to yield plasmid DNA for each library. Sequencing was performed by Source Bioscience (Nottingham).

Shuffling by overlap extension PCR:

After rounds 1 and 2 of evolution, beneficial mutations were combined by DNA shuffling of fragments generated by overlap extension PCR. Primers were designed that encoded either the parent amino acid or the identified mutation. These primers were used to generate short fragments that were gel-purified and mixed for assembly of the full length gene by overlap extension PCR. Final full length genes contain all possible combinations of mutations at specified positions. Genes were cloned as described above.

Library screening:

For protein expression and screening, all transfer and aliquoting steps were performed using Hamilton liquid-handling robots. Chemically competent *E. coli* BL21(DE3) cells harbouring pEVOL_pBpA/$tRNA_{CUA}$ were transformed with the appropriate library plasmids. Freshly transformed colonies were used to inoculate 180 µL of 2xYT medium supplemented with 50 µg mL^{-1} kanamycin and 25 µg mL^{-1} chloramphenicol in Corning® Costar® 96-well microtiter round bottom plates. Each plate contained 6 freshly transformed clones of the parent template and 2 clones containing pET-29b(+)_Ent1.0 as internal references. Plates were incubated overnight at 30 °C, 80 % humidity in a shaking incubator at 900 r.p.m. 20 µL of overnight culture was used to inoculate 480 µL 2xYT medium supplemented with 50 µg mL^{-1} kanamycin, 25 µg mL^{-1} chloramphenicol and 1 mM BpA which was added as a 1 M stock dissolved in 1 M NaOH. The cultures were incubated at 30 °C, 80 % humidity and 900 r.p.m. until an OD_{600} of ~0.6. Protein expression was induced by the addition of L-arabinose to a final concentration of 0.05% and IPTG to a final concentration of 0.1 mM. Induced plates were incubated for 20 h at 30 °C, 80 % humidity and 900 r.p.m. Cells were harvested by centrifugation at 2,900 *g* for 5 min. The supernatant was discarded and the pelleted cells were resuspended in 400 µL of PBS lysis buffer (137 mM NaCl; 2.7 mM KCl; 10 mM Na_2HPO_4; 1.8 mM KH_2PO_4, pH 7.4, 1.0 mg mL^{-1} lysozyme, 0.5 mg mL^{-1} polymixin B and 1 µg mL^{-1} DNase I) and incubated for 2 h at 30 °C, 80 % humidity with shaking at 900 r.p.m. Cell debris was removed by centrifugation at 2,900 *g* for 5 min.

Rounds 1&2:

A 75 µl volume of clarified lysate was transferred to 96-well polypropylene microtiter plates containing 25 µl of 1.2 mM substrate **1** in PBS buffer pH 7.4 with 20% DMSO as a cosolvent. Samples were irradiated at 365 nm in a UV curing LED oven (equipped with 365 nm & 395 nm LEDs, UV intensity 750 mW cm^{-2}, LED module size 100 x 100, NovaChem), with pulsing irradiation (10 seconds on, 10 seconds off) at 4 °C for a total irradiation time of 30 minutes at 100% intensity. Reactions were quenched with the addition of 100 µl of acetonitrile, the plates heat sealed, and incubated for a further 1 h at 30 °C, 80% humidity, and 900 r.p.m. Precipitated proteins were removed by centrifugation at 2,900 *g* for 10 min. A 100 µl volume of the clarified reaction mixture was transferred to 96-well polypropylene microtiter plates and heat-sealed with pierceable foil. Reactions were evaluated by UPLC analysis.

*Round 3: Improvement of EnT1.3 Y121F activity towards substrate **13**:*

A 75 µl volume of clarified lysate was transferred to 96-well polypropylene microtiter plates containing 25 µl of 1.2 mM substrate **13** in PBS buffer pH 7.4 with 20% DMSO as a cosolvent. Samples were irradiated at 365 nm in a UV curing LED oven (equipped with 365 nm & 395 nm LEDs, UV intensity 750 mW cm^{-2}, LED module size 100 x 100, NovaChem), with pulsing irradiation (10 seconds on, 10 seconds off) at 4 °C for a total irradiation time of 30 minutes at 100% intensity. Reactions were quenched with the addition of 100 µl of acetonitrile, the plates heat sealed, and incubated for a further 1 h at 30 °C, 80% humidity, and 900 r.p.m. Precipitated proteins were removed by centrifugation at 2,900 *g* for 10 min. A 100 µl volume of the clarified reaction mixture was transferred to 96-well polypropylene microtiter plates and heat-sealed with pierceable foil. Reactions were evaluated by UPLC analysis.

Following each round, the most active variants were rescreened as purified proteins and evaluated by both Ultra Performance Liquid Chromatography (UPLC) and Supercritical Fluid Chromatography (SFC) analysis. Proteins were expressed and purified as described above with the exception that starter cultures were inoculated from glycerol stocks prepared from the original library plate overnight cultures.

General procedure for analytical scale biotransformations:

96-well microtiter round bottom polypropylene plates were used for biotransformations, using HD clear high-performance tape (Duck), 3-inch x 54.6-yard roll to seal the samples. Biotransformations were performed at 4 °C using 0.4 mM substrate **1** and the relevant biocatalyst (20 µM) in PBS buffer pH 7.4 with 5% DMSO as a cosolvent. Samples were irradiated at 365 or 395 nm in a UV curing LED oven (NovaChem), 23 cm below the LED array (unless stated otherwise). Instrument settings: 100% intensity, 750 mW cm^{-2}, 10 seconds on/off pulse. Conditions for substrate scope characterisation are detailed in Supplementary Information Table S3. Reactions were evaluated by UPLC analysis.

Anaerobic biotransformations:

For anaerobic biotransformations samples of EnT1.3 and substrate were incubated in a glovebox overnight on ice to ensure complete removal of oxygen. Reactions were made up in the glovebox in glass vials (final volume of 500 µL) using 2.5 mol% (10 µM) EnT1.3 in PBS (pH 7.4) with 5% DMSO as a co-solvent. 25 µL samples were taken at 10, 20, 30, 60 and 90 minutes and quenched with 2 volumes MeCN. Reactions were evaluated by UPLC analysis.

Total turnover numbers:

Total turnover numbers achieved by EnT1.3 were determined as follows. EnT1.3 (0.2 or 1.5 mol%)-catalysed biotransformations were performed in glass vials using **1** (800 µM) in PBS (pH 7.4) with 10% DMSO cosolvent (Extended Data Figure 7) in a 1 mL volume. Reactions were performed under general conditions and samples were taken at 10, 20, 30, 40, 50, 60, 90, 120, 150, 180 and 210 minutes by sampling 50 µL of the reaction and quenching with 2 volumes of MeCN. Reactions were evaluated by UPLC analysis.

EnT1.3 temperature profile:

Biotransformations were performed at 4 °C and room temperature in glass vials using 2.25 µM of EnT1.3 and 300 µM of substrate **1** in PBS buffer with 5% DMSO as a co-solvent (final volume of 500 µL). For reactions at 4 °C, all reaction components were incubated in a cold room maintained at 4 °C for 30 minutes prior to running reactions. For both temperatures reactions were run using 100% intensity

irradiation at 365 nm with 10 seconds on/ 10 seconds off intervals and 25 µL samples were taken at 10, 20, 30, 40, 50, 60, 90 and 120 minutes. Reactions were evaluated by UPLC analysis.

EnT1.3 cosolvent tolerance:

To investigate cosolvent tolerance, analytical-scale biotransformations were performed using **1** (400 µM) and EnT1.3 (7.5 µM) in 100 µL PBS buffer (pH 7.4) with the stated concentration of MeCN or DMSO, for a total irradiation time of 30 minutes at 100% intensity at 365 nm with 10 seconds on/ 10 seconds off intervals at 4 °C (Supplementary Information, Table S6). Reactions were run in a 96-well plate and evaluated by UPLC analysis.

Photodamage biotransformations:

To investigate the effects of photodamage, 1 mL aliquots of 30 µM enzyme in PBS (pH 7.4) were pre-irradiated for 90 minutes (10 seconds on/off pulse at 365 nm) in glass vials at 4 °C before performing reactions. Control aliquots of enzyme were incubated in the dark at 4 °C. Light exposed and non-light exposed protein samples (DA_20_00, EnT1.0 and EnT1.3) were analysed by SDS-PAGE (4-20% Mini-PROTEAN® TGX™ Precast Protein Gel, Bio-Rad) running at 100 volts for 90 minutes and stained using InstantBlue™ Coomassie Stain (abcam) (Extended Data Figure 5). Biotransformations were established with 15 µM enzyme and **1** (400 µM) in PBS (pH 7.4) with 5% DMSO cosolvent and ran at 4 °C using 100% light intensity for 30 minutes irradiation (10 seconds on/off pulse) at 365 nm. Reactions were run in a 96-well plate with 100 µL volume. Reactions were evaluated by UPLC analysis.

EnT1.3 substrate concentration rate profile:

To investigate the effect of substrate concentration on the rate of reaction with EnT1.3, biotransformations were performed using 1 µM EnT1.3 and a range of substrate concentrations (0 µM, 20 µM, 50 µM, 80 µM, 100 µM, 125 µM, 150 µM, 200 µM, 250 µM, 300 µM) in PBS buffer (pH 7.4) with 5 % DMSO as a co-solvent. Reactions were run in a 96-well plate with 250 µL volume and irradiated at 4 °C (10 seconds on/off pulse at 365 nm). Time points were taken at 4 min, 8 min, 12 min, and 16 min of irradiation by sampling 50 µL of the reaction and quenching with 2 volumes of MeCN. Samples were analysed by UPLC analysis. The initial rate v_0 at each substrate concentration was calculated using the slope of the time course.

EnT1.3 light intensity rate profile:

To investigate the effect of light intensity on the rate of reaction with EnT1.3, biotransformations were performed in 2 mL MS glass vials using 1 µM EnT1.3 and 400 µM **1** in PBS buffer (pH 7.4) with 5% DMSO as a co-solvent (500 µL total reaction volume). Reactions were positioned at a 3 cm distance from the LED array and irradiated as described at varying LED intensities and time points taken at 2 min, 4 min, 6 min, 8 min and 10 min for 30% and 40%, and 4 min, 8 min, 12 min, 16 min and 20 min for 10% and 20% and analysed by UPLC analysis. The reaction rate at each light intensity was calculated using the slope of the time course (as an average of triplicate measurements), which remained linear in each case.

Preparative scale biotransformation:

Substrate **1** (12 mg) was dissolved to a concentration of 400 µM in PBS buffer (pH 7.4) with 5% DMSO as a co-solvent (140 mL reaction volume) with 10 µM EnT1.3 (2.5 mol%). The solution was irradiated as described at 365 nm for a total reaction time of 2 h in a Pyrex dish (22 cm diameter, solution path length = 0.37 cm). Once full conversion was reached (as monitored by UPLC) the solution was transferred to a separatory funnel and extracted with 3 x 20 mL ethyl acetate and the combined organic layers were washed with 3 x 20 mL brine, dried over $MgSO_4$, filtered and concentrated *in vacuo* to afford optically pure **1a** along with its minor regioisomer **1b** (9:1 r.r., 11.4 mg, 95%), which required no further purification.

Bimolecular biotransformations:

Biotransformations were performed using 100 µM EnT1.3 (5 mol%), 2 mM 2-quinolone and 50 mM of methyl vinyl ketone or ethyl vinyl ketone in 100 µL PBS buffer (pH 7.4) with 5% DMSO as a co-solvent. Reactions were run in a 96-well plate for a total irradiation time of 4 h at 100% intensity at 395 nm with 10 seconds on/ 10 seconds off intervals at 4 °C, quenched with 1 volume MeCN and evaluated by UPLC and chiral HPLC analysis.

Biotransformations with Exogenous Benzophenone using EnT1.3 BpA173A:

Biotransformations were performed using 10 µM of EnT1.3 BpA173A, 10 µM Benzophenone (taken from a 1 mM stock in MeCN) and 400 µM of substrate **1** in 100 µL PBS buffer (pH 7.4) with 5% DMSO as a co-solvent. Reactions were run in a 96-well plate for a total irradiation time of 60 minutes at 100% intensity at 365 nm with 10 seconds on/ 10 seconds off intervals at 4 °C, quenched with 1 volume MeCN and evaluated by UPLC and chiral SFC analysis.

Chromatographic analysis:

For UPLC analysis, reactions were quenched at the stated time points with the addition of 1 volume acetonitrile. Samples were shaken at 900 r.p.m for 1h and precipitated proteins were removed by centrifugation (2,900 *g* for 10 minutes). For SFC and chiral HPLC analysis, the substrates and products were transferred into 1.5 mL microcentrifuge tubes and extracted with 3 volumes of ethyl acetate. Precipitated proteins were removed by centrifugation (14,000 *g* for 15 minutes), the organic phase was separated and directly injected onto the SFC.

UPLC analysis was performed on a 1290 Infinity II Agilent LC system with a Kinetex® 5 µm XB-C18 100 Å LC Column, 50 x 2.1 mm (Phenomenex). Peaks were assigned by comparison to chemically synthesized standards and the peak areas were integrated using Agilent OpenLab software. The separation methods for all substrate(s)/product(s) and extinction coefficients used to calculate the conversion are reported in Supplementary Information, Table S8.

Chiral analysis was performed using either an SFC 1290 Infinity II Agilent system or a HPLC 1260 Agilent system. Enantiomers of all reaction products **1a**-**12a** were separated using a Diacel 87S82 CHIRALPAK ® IG-3 SFC column, 3 mm, 50 mm, 3 µm. For all adducts (**1a**–**13a)** the major stereoisomer formed in the biotransformations was assigned based on an analogy to EnT1.3-derived (-)-**1a**. Peaks were assigned by comparison to chemically synthesized standards and peak areas were integrated using Agilent OpenLabs software. Separation methods for all substrate(s)/product(s) enantiomers used to determine enantiomeric excess are reported in Supplementary Table S9 for SFC methods, and Supplementary Table S10 for chiral HPLC methods.

Laser Pulse Experiments:

Laser photoexcitation experiments were carried out at 4°C using an Edinburgh Instruments LP980 Transient Absorption Spectrometer. Samples contained 50 µM benzophenone, Ent1.0 or Ent1.3 in PBS buffer (pH 7.4) and O_2 was removed where necessary by incubation in an anaerobic glovebox (Belle Technology) for 4 hours. Triplet formation was initiated by excitation at 355 nm (~50 mJ), using the 3rd harmonic of a Q-switched Nd-YAG laser (NT342B, EKSPLA) in a cuvette of 1 cm pathlength. Time-dependent absorbance difference spectra were recorded with an ICCD detector using a gate width of 100ns and 50 averages. Kinetic transients were recorded using 50 averages at the specified wavelengths with the detection system (comprising probe light, sample, monochromator and photomultiplier tube detector) at right angles to the incident laser beam. Lifetimes were measure by fitting to a double exponential function using Origin Pro 9.1 software.

Chemical Procedures:

General Procedure 1: Synthesis of 4-(allyloxy)-quinolones* 1-5, 13. Quinoline-2,4-diol (500 mg, 3.10 mmol, 1 eq.) was dissolved in 10 mL of dry DMF with K_2CO_3 (857 mg, 6.20 mmol, 2 eq.) and stirred at 90°C for 1 h under nitrogen. Subsequently, the corresponding alkenyl bromide (4.65 mmol, 1.5 eq.) was added dropwise, and the solution was stirred overnight at 90°C. The reaction was quenched by addition of aqueous 1M HCl (30 mL) and then extracted with ethyl acetate (3 x 100 mL). The combined organic layers were washed with brine (2 x 50 mL), dried over $MgSO_4$, filtered and the solvent removed *in vacuo* to give the crude product.

*Substrates **5** and **13** were synthesised in the same manner using and **4**-h**ydroxy**-**3**-methylquinolin-2(1H)-one and 4-hydroxy-1-methylquinolin-2(1H)-one as the starting material, respectively.

General Procedure 2[9]: Synthesis of 4-((allyloxy)methyl)quinolones 10-12. A solution of the corresponding allylic alcohol (2.73 mmol, 1.3 eq.) in 3.5 mL of dry THF was added to a suspension of sodium hydride (60% in paraffin oil, 185 mg, 4.62 mmol, 2.2 eq.) in 3.5 mL of dry THF at 0°C. The reaction mixture was stirred at 0°C for 2 h and then heated to reflux for a further 2 h. After cooling to room temperature, the solution was added dropwise to a stirring suspension of 4-bromomethyl-2(1*H*)-quinolinone (500 mg, 2.10 mmol, 1 eq.) in 3 mL dry THF at 0°C. Subsequently, the reaction mixture was stirred for 6 h at room temperature. The reaction was quenched by addition of aqueous 1M HCl (30 mL) and then extracted with ethyl acetate (3 x 100 mL). The combined organic layers were washed with brine (2 x 50 mL), dried over $MgSO_4$, filtered and the solvent removed *in vacuo* to give the crude product.

General Procedure 3[15]: Synthesis of 4-(pent-4-en-1-yl)quinolones 6-9 2-hydroxy-4-methylquinoline (500 mg, 3.14 mmol, 1 eq.) was suspended in 17.5 mL dry THF, cooled to 0°C and treated dropwise with *n*-butyl lithium (2.5M in hexane, 2.76 mL, 6.9 mmol, 2.2 eq.) under a nitrogen atmosphere. The dark red solution was stirred at room temperature for 2 h, cooled to -78°C and treated with tetrabutylammonium iodide (872 mg, 2.36 mmol, 0.75 eq.) and the corresponding alkenyl bromide (6.34 mmol, 2.02 eq.) was added subsequently. The yellow solution was stirred at room temperature under a nitrogen atmosphere for a further 3 h, cooled to 0°C and quenched by slow addition of 1M HCl (30 mL). The resulting solution was extracted with dichloromethane (3 x 100 mL). The combined organic layers were washed with aqueous $NaHCO_3$ (60%, 50 mL) and brine (2 x 50 mL), dried over $MgSO_4$, filtered and the solvent removed *in vacuo* to give the crude product.

General procedure 4: Synthesis of intramolecular [2+2]-cycloaddition product standards 1-13(a/b). The corresponding quinolones **1-13** (100 mg) were dissolved in acetonitrile to a concentration of 10 mM and degassed by bubbling nitrogen through the solution for 30 minutes. The solution was irradiated at $\lambda = 300$ nm at room temperature until full conversion was achieved (as monitored by TLC). The solvent was removed *in vacuo* to give the crude product.

General procedure 5: Synthesis of bimolecular [2+2]-cycloaddition product standards 14 and 15. 2-Quinolone (100 mg) was dissolved in acetonitrile to a concentration of 10 mM with 50 mol% thioxanthone and degassed as described. Once dissolved and degassed the corresponding vinyl ketone (10 eq) was added and the solution was irradiated at $\lambda = 395$nm at 4°C until full conversion was achieved (as monitored by TLC). The solvent was removed *in vacuo* to give the crude product.

4-(but-3-en-1-yloxy)quinolin-2(1H)-one (1). The crude product was purified by flash chromatography (1:1 ethyl acetate:cyclohexane) to give the product as a colourless solid (407 mg, 61%). EI-MS *m/z* = 216 $[M + H]^+$. ^{1}H NMR (400 MHz, $CDCl_3$) δ 12.49 (s, 1H, *NH*), 7.90 (d, *J* = 8.1 Hz, 1H, *Ph*), 7.50 (t, *J* = 7.6 Hz, 1H, *Ph*), 7.43 (d, *J* = 8.2 Hz, 1H, *Ph*), 7.19 (t, *J* = 7.6 Hz, 1H, *Ph*), 6.02 (s, 1H, *CH*), 5.94 (ddt, *J* = 16.9, 10.1, 6.7 Hz, 1H, *CH*), 5.23 (dq, *J* = 17.2, 1.6 Hz, 1H, *CH*), 5.16 (dq, *J* = 10.3, 1.4 Hz,

1H, *CH*), 4.17 (t, *J* = 6.5 Hz, 2H, *CH₂*), 2.67 (q, *J* = 6.4 Hz, 2H, *CH₂*); ^{13}C NMR (101 MHz, $CDCl_3$) δ 166.41, 164.28, 138.57, 133.84, 131.29, 122.86, 122.29, 117.83, 116.34, 115.75, 96.42, 67.92, 33.18.

4-(pent-4-en-1-yloxy)quinolin-2(1H)-one (2). The crude product was purified by flash chromatography (1:1 ethyl acetate:cyclohexane) to give the product as a colourless solid (448 mg, 63%). EI-MS *m/z* = 230 $[M + H]^+$. ^{1}H NMR (400 MHz, $CDCl_3$) δ 12.55 (s, 1H, *NH*), 7.91 (dd, *J* = 8.1, 1.4 Hz, 1H, *Ph*), 7.50 (ddd, *J* = 8.4, 7.0, 1.4 Hz, 1H, *Ph*), 7.43 (dd, *J* = 8.3, 1.2 Hz, 1H, *Ph*), 7.19 (ddd, *J* = 8.2, 7.0, 1.3 Hz, 1H, *Ph*), 6.01 (s, 1H, *CH*), 5.86 (ddt, *J* = 16.9, 10.2, 6.7 Hz, 1H, *CH*), 5.13 – 5.00 (m, 2H, *CH₂*), 4.13 (t, *J* = 6.3 Hz, 2H, *CH₂*), 2.31 (q, *J* = 7.4 Hz, 2H, *CH₂*), 2.01 (p, *J* = 6.6 Hz, 2H, *CH₂*).; ^{13}C NMR (101 MHz, $CDCl_3$) δ 166.49, 164.36, 138.59, 137.35, 131.23, 122.81, 122.23, 116.37, 115.82, 115.78, 96.41, 68.08, 30.24, 27.93.

4-((4-methylpent-3-en-1-yl)oxy)quinolin-2(1H)-one (3). The crude product was purified by flash chromatography (1:2 ethyl acetate:cyclohexane) to give the product as a colourless solid (422 mg, 56%). EI-MS *m/z* = 244 $[M + H]^+$. ^{1}H NMR (400 MHz, $CDCl_3$) δ 11.96 (s, 1H, *NH*), 7.83 (d, *J* = 8.1 Hz, 1H, *Ph*), 7.48 (t, *J* = 8.4 Hz, 1H, *Ph*), 7.41 (d, *J* = 8.2 Hz, 1H, *Ph*), 7.18 (t, *J* = 7.5 Hz, 1H, *Ph*), 5.92 (s, 1H, *CH*), 5.19 (t, *J* = 7.1 Hz, 1H, *CH*), 3.91 (t, *J* = 6.7 Hz, 2H, *CH₂*), 2.52 (q, *J* = 6.9 Hz, 2H, *CH₂*), 1.74 (s, 3H, *CH₃*), 1.69 (s, 3H, *CH₃*); ^{13}C NMR (101 MHz, $CDCl_3$) δ 166.07, 164.63, 138.13, 135.06, 131.30, 122.86, 122.47, 119.10, 116.42, 115.83, 96.26, 68.59, 27.78, 25.90, 18.06.

4-(allyloxy)quinolin-2(1H)-one (4). The crude product was purified by flash chromatography (1:2 ethyl acetate:cyclohexane) to give the product as a colourless solid (374 mg, 60%). EI-MS *m/z* = 202 $[M + H]^+$. ^{1}H NMR (400 MHz, $CDCl_3$) δ 12.01 (s, 1H, *NH*), 7.97 (d, *J* = 6.7 Hz, 1H, *Ph*), 7.53 (t, *J* = 7.0 Hz, 1H, *Ph*), 7.42 (d, *J* = 8.0 Hz, 1H, *Ph*), 7.23 (t, 1H, *Ph*), 6.12 (ddt, *J* = 17.3, 10.6, 5.3 Hz, 1H, *CH*), 6.05 (s, 1H, *CH*), 5.52 (dq, *J* = 17.4, 1.6 Hz, 1H, *CH*), 5.40 (dt, *J* = 10.5, 1.3 Hz, 1H, *CH*), 4.70 (d, *J* = 5.4 Hz, 2H, *CH₂*); ^{13}C NMR (101 MHz, $CDCl_3$) δ 164.20, 138.33, 131.53, 131.51, 123.02, 122.62, 119.08, 116.39, 115.87, 96.78, 69.58, 27.05.

4-(but-3-en-1-yloxy)-3-methylquinolin-2(1H)-one (5). The crude product was purified by flash chromatography (1:1 EtOAc:toluene) to give a white solid (49 mg, 46%). EI-MS *m/z* = 230 $[M + H]^+$. ^{1}H NMR (400 MHz, $CDCl_3$) δ 12.01 (s, 1H, *NH*), 7.79 (d, *J* = 7.3 Hz, 1H, *Ph*), 7.49 (t, *J* = 7.6 Hz, 1H, *Ph*), 7.44 (d, *J* = 8.6 Hz, 1H, *Ph*), 7.23 (t, *J* = 8.2 Hz, 1H, *Ph*), 5.98 (ddt, *J* = 17.0, 10.2, 6.8 Hz, 1H, *CH*), 5.28 – 5.15 (m, 2H, *CH₂*), 4.09 (t, *J* = 6.7 Hz, 2H, *CH₂*), 2.65 (q, *J* = 6.8 Hz, 2H, *CH₂*), 2.25 (s, 3H, *CH₃*). ^{13}C NMR (101 MHz, $CDCl_3$) δ 166.23, 161.75, 137.16, 134.20, 130.18, 122.87, 122.58, 118.55, 117.88, 117.74, 116.21, 73.23, 34.86, 10.33.

4-(pent-4-en-1-yl)quinolin-2(1H)-one (6). The crude product was purified by flash chromatography (1:1 ethyl acetate:cyclohexane) to give the product as a colourless solid (469 mg, 70%). EI-MS *m/z* = 214 $[M + H]^+$. ^{1}H NMR (400 MHz, $CDCl_3$) δ 12.85 (s, 1H, *NH*), 7.71 (d, *J* = 8.1 Hz, 1H, *Ph*), 7.55 – 7.45 (m, 2H, *Ph*), 7.23 (td, *J* = 8.6, 4.5 Hz, 1H, *Ph*), 6.61 (s, 1H, *CH*), 5.85 (ddt, *J* = 17.0, 10.2, 6.6 Hz, 1H, *CH*), 5.13 – 4.99 (m, 2H, *CH₂*), 2.87 (t, *J* = 7.7 Hz, 2H, *CH₂*), 2.21 (q, *J* = 7.2 Hz, 1H, *CH*), 1.84 (p, *J* = 7.5 Hz, 2H, *CH₂*); ^{13}C NMR (101 MHz, $CDCl_3$) δ 164.68, 153.26, 138.75, 137.91, 130.52, 124.21, 122.62, 119.95, 119.52, 117.12, 115.64, 33.49, 31.64, 28.03.

4-(hex-5-en-1-yl)quinolin-2(1H)-one (7). The crude product was purified by flash chromatography (1:1 ethyl acetate:cyclohexane) to give the product as a colourless solid (486 mg, 68%). EI-MS *m/z* = 228 $[M + H]^+$. ^{1}H NMR (400 MHz, $CDCl_3$) δ 12.77 (s, 1H, *NH*), 7.72 (d, *J* = 8.1 Hz, 1H, *Ph*), 7.55 – 7.45 (m, 2H, *Ph*), 7.29 – 7.18 (m, 1H, *Ph*), 6.61 (s, 1H, *CH*), 5.81 (ddt, *J* = 16.9, 10.2, 6.7 Hz, 1H, *CH*), 5.07 – 4.93 (m, 2H, *CH₂*), 2.87 (t, *J* = 7.7 Hz, 2H, *CH₂*), 2.18 – 2.08 (m, 2H, *CH₂*), 1.81 – 1.67 (m, 2H, *CH₂*), 1.61 – 1.49 (m, 2H, *CH₂*); ^{13}C NMR (101 MHz, $CDCl_3$) δ 164.61, 153.58, 138.66, 138.50, 130.56, 124.24, 122.70, 120.04, 119.31, 117.16, 114.99, 33.62, 32.23, 28.82, 28.37.

4-(5-methylhex-4-en-1-yl)quinolin-2(1H)-one (8). The crude product was purified by flash chromatography (1:1 ethyl acetate:cyclohexane) to give the product as a colourless solid (500 mg, 66%). EI-MS *m/z* = 242 $[M + H]^+$. ^{1}H NMR (400 MHz, $CDCl_3$) δ 12.53 (s, 1H, *NH*), 7.72 (d, *J* = 7.8 Hz, 1H, *Ph*), 7.50 (t, *J* = 7.8 Hz, 1H, *Ph*), 7.48 (d, *J* = 6.2 Hz, 1H, *Ph*), 7.24 (t, *J* = 6.3 Hz, 1H, *Ph*), 6.62 (s, 1H, *CH*), 5.17 (t, *J* = 7.2 Hz, 1H, *CH*), 2.86 (t, *J* = 8.1 Hz, 2H, CH_2), 2.14 (q, *J* = 7.2 Hz, 2H, CH_2), 1.78 (p, *J* = 7.5 Hz, 2H, CH_2), 1.72 (s, 3H, CH_3), 1.62 (s, 3H, CH_3); ^{13}C NMR (101 MHz, $CDCl_3$) δ 164.47, 153.78, 138.60, 132.83, 130.57, 124.33, 123.69, 122.72, 120.10, 119.32, 117.09, 31.89, 29.13, 27.87, 25.89, 17.98.

4-(4-methylpent-4-en-1-yl)quinolin-2(1H)-one (9). The crude product was purified by flash chromatography (1:1 ethyl acetate:cyclohexane) to give the product as a colourless solid (465 mg, 65%). EI-MS *m/z* = 228 $[M + H]^+$. ^{1}H NMR (400 MHz, $CDCl_3$) δ 12.58 (s, 1H, *NH*), 7.72 (d, *J* = 8.1 Hz, 1H, *Ph*), 7.51 (t, *J* = 7.4 Hz, 1H, *Ph*), 7.48 (d, *J* = 8.1 Hz, 1H, *Ph*), 7.24 (d, *J* = 7.4 Hz, 1H, *Ph*), 6.63 (s, 1H, *CH*), 4.78 (s, 1H, *CH*), 4.74 (s, 1H, *CH*), 2.87 (t, *J* = 7.9 Hz, 2H, CH_2), 2.17 (t, *J* = 7.5 Hz, 2H, CH_2), 1.89 (p, *J* = 7.5 Hz, 2H, CH_2), 1.75 (s, 3H, CH_3). ^{13}C NMR (101 MHz, $CDCl_3$) δ 164.71, 153.29, 144.98, 138.76, 130.50, 124.19, 122.59, 119.97, 119.54, 117.07, 110.81, 37.51, 31.77, 26.68, 22.51.

4-((allyloxy)methyl)quinolin-2(1H)-one (10). The crude product was purified by flash chromatography (1:1 ethyl acetate:cyclohexane) to give the product as a colourless solid (420 mg, 93%). EI-MS *m/z* = 216 $[M + H]^+$. ^{1}H NMR (400 MHz, $CDCl_3$) δ 12.42 (s, 1H, *NH*), 7.68 (d, *J* = 6.9 Hz, 1H, *Ph*), 7.53 (t, *J* = 6.9 Hz, 1H, *Ph*), 7.48 (d, *J* = 6.8 Hz, 1H, *Ph*), 7.24 (t, *J* = 6.7 Hz, 1H, *Ph*), 6.89 (s, 1H, *CH*), 5.98 (ddt, *J* = 17.3, 10.8, 5.5 Hz, 1H, *CH*), 5.37 (dq, *J* = 17.2, 1.6 Hz, 1H, *CH*), 5.26 (dq, *J* = 10.4, 1.4 Hz, 1H, *CH*), 4.79 (s, 2H, CH_2), 4.16 (dt, *J* = 5.5, 1.5 Hz, 2H, CH_2); ^{13}C NMR (101 MHz, $CDCl_3$) δ 164.33, 148.89, 138.49, 134.14, 130.83, 123.87, 122.94, 118.84, 118.61, 117.93, 116.96, 72.01, 68.60.

4-(((2-methylallyl)oxy)methyl)quinolin-2(1H)-one (11). The crude product was purified by flash chromatography (1:1 ethyl acetate:cyclohexane) to give the product as a colourless solid (366 mg, 73%). EI-MS *m/z* = 230 $[M + H]^+$. ^{1}H NMR (400 MHz, $CDCl_3$) δ 12.45 (s, 1H, *NH*), 7.68 (d, *J* = 7.5 Hz, 1H, *Ph*), 7.52 (t, *J* = 7.5 Hz, 1H, *Ph*), 7.48 (d, *J* = 6.7 Hz, 1H, *Ph*), 7.23 (t, *J* = 7.5 Hz, 1H, *Ph*), 6.89 (s, 1H, *CH*), 5.05 (s, 1H, *CH*), 4.97 (s, 1H, *CH*), 4.77 (s, 2H, CH_2), 4.05 (s, 2H, CH_2), 1.79 (s, 3H, CH_3); ^{13}C NMR (101 MHz, $CDCl_3$) δ 164.48, 148.86, 141.67, 138.53, 130.76, 123.82, 122.84, 118.85, 118.57, 116.92, 113.06, 74.98, 68.36, 19.65.

4-(((3-methylbut-2-en-1-yl)oxy)methyl)quinolin-2(1H)-one (12). The crude product was purified by flash chromatography (1:1 ethyl acetate:cyclohexane) to give the product as a colourless solid (408 mg, 80%). EI-MS *m/z* = 244 $[M + H]^+$. ^{1}H NMR (400 MHz, $CDCl_3$) δ 12.35 (s, 1H, *NH*), 7.72 (d, *J* = 6.9 Hz, 1H, *Ph*), 7.53 (t, *J* = 7.6 Hz, 1H, *Ph*), 7.47 (d, *J* = 6.9 Hz, 1H, *Ph*), 7.25 (t, *J* = 7.4 Hz, 1H, *Ph*), 6.87 (s, 1H, *CH*), 5.43 (t, *J* = 6.9 Hz, 1H, *CH*), 4.76 (s, 2H, CH_2), 4.12 (d, *J* = 6.9 Hz, 2H, CH_2), 1.78 (s, 3H, CH_3), 1.69 (s, 3H, CH_3); ^{13}C NMR (101 MHz, $CDCl_3$) δ 164.29, 149.26, 138.46, 138.29, 130.82, 124.08, 122.96, 120.55, 118.99, 118.79, 116.93, 68.54, 67.49, 25.96, 18.28.

4-(but-3-en-1-yloxy)-1-methylquinolin-2(1H)-one (13). The crude product was purified by flash chromatography (1:2 ethyl acetate:cyclohexane) to give the product as a yellow solid (445 mg, 68%). EI-MS *m/z* = 229 $[M + H]^+$. ^{1}H NMR (400 MHz, $CDCl_3$) δ 7.96 (dd, *J* = 8.0, 1.6 Hz, 1H, *Ph*), 7.56 (ddd, *J* = 8.6, 7.1, 1.6 Hz, 1H, *Ph*), 7.35 – 7.28 (m, 1H, *Ph*), 7.21 (ddd, *J* = 8.1, 7.2, 1.1 Hz, 1H, *Ph*), 6.00 (s, 1H, *CH*), 5.92 (ddt, *J* = 17.0, 10.3, 6.7 Hz, 1H, *CH*), 5.22 (dq, *J* = 17.2, 1.6 Hz, 1H, *CH*), 5.15 (dq, *J* = 10.2, 1.4 Hz, 1H, *CH*), 4.12 (t, *J* = 6.5 Hz, 2H, CH_2), 3.65 (s, 3H, CH_3), 2.64 (qt, *J* = 6.5, 1.4 Hz, 2H, CH_2). ^{13}C NMR (101 MHz, $CDCl_3$) δ 163.92, 161.86, 139.88, 133.89, 131.28, 123.49, 121.70, 117.74, 116.68, 114.10, 97.06, 67.69, 33.18, 29.14.

3,3a,4,4a-tetrahydro-2H-furo[2',3':2,3]cyclobuta[1,2-c]quinolin-5(6H)-one (1a, straight-product). The crude product was purified by flash chromatography (1:1 ethyl acetate:cyclohexane) to give the product as a colourless solid (60 mg, 60%). EI-MS *m/z* = 216 $[M + H]^+$. ^{1}H NMR (400 MHz,

$CDCl_3$) δ 9.39 (s, 1H, *NH*), 7.27 (dd, J = 7.9, 1.6 Hz, 1H, *Ph*), 7.20 (td, J = 7.6, 1.6 Hz, 1H, *Ph*), 7.03 (td, J = 7.5, 1.2 Hz, 1H, *Ph*), 6.82 (d, J = 8.0 Hz, 1H, *Ph*), 4.45 (ddd, J = 9.2, 7.8, 1.4 Hz, 1H, *CH*), 4.22 (ddd, J = 10.9, 9.2, 5.6 Hz, 1H, *CH*), 3.36 (ddd, J = 11.3, 6.9, 1.5 Hz, 1H, *CH*), 2.96 (td, J = 8.7, 5.2 Hz, 1H, *CH*), 2.47 – 2.36 (m, 1H, *CH*), 2.25 – 2.06 (m, 2H, CH_2), 1.83 (dd, J = 12.8, 5.5 Hz, 1H, *CH*); ^{13}C NMR (101 MHz, $CDCl_3$) δ 172.38, 136.20, 129.37, 126.44, 124.01, 123.61, 115.84, 83.44, 68.68, 46.83, 42.46, 32.45, 26.87.

2,3,4,4a-tetrahydro-4,10b-methanopyrano[3,2-c]quinolin-5(6H)-one (1b, crossed-product). The crude product was purified by flash chromatography (1:1 ethyl acetate:cyclohexane) to give the product as a colourless solid (20 mg, 20%). EI-MS m/z = 216 $[M + H]^+$. ^{1}H NMR (400 MHz, $CDCl_3$) δ 9.36 (s, 1H, *NH*), 7.39 (dd, J = 7.4, 1.7 Hz 1H, *Ph*), 7.20 (td, J = 7.6, 1.6 Hz, 1H, *Ph*), 7.06 (t, J = 7.5 Hz, 1H, *Ph*), 6.86 (d, J = 7.8 Hz, 1H, *Ph*), 4.46 – 4.35 (m, 1H, *CH*), 4.32 – 4.21 (m, 1H, *CH*), 3.12 (ddd, J = 6.2, 4.2, 2.4 Hz, 1H, *CH*), 2.91 (d, J = 7.9 Hz, 1H, *CH*), 2.62 – 2.53 (m, 1H, *CH*), 2.46 – 2.33 (m, 1H, *CH*), 2.31 – 2.21 (m, 1H, *CH*), 2.18 (dd, J = 11.0, 8.0 Hz, 1H, *CH*); ^{13}C NMR (101 MHz, $CDCl_3$) δ 173.19, 135.46, 128.83, 125.22, 123.98, 123.84, 115.65, 80.20, 60.92, 51.23, 36.94, 36.52, 31.69.

2,3,4,4a,5,5a-hexahydropyrano[2',3':2,3]cyclobuta[1,2-c]quinolin-6(7H)-one (2a, straight-product). The crude product was purified by flash chromatography (1:2 ethyl acetate:cyclohexane) to give the product as a colourless solid (71 mg, 71%). EI-MS m/z = 230 $[M + H]^+$. ^{1}H NMR (400 MHz, $CDCl_3$) δ 8.70 (s, 1H, *NH*), 7.45 (dd, J = 7.8, 1.5 Hz, 1H, *Ph*), 7.25 (td, J = 7.7, 1.5 Hz, 1H, *Ph*), 7.11 (td, J = 7.5, 1.2 Hz, 1H, *Ph*), 6.79 (dd, J = 8.0, 1.2 Hz, 1H, *Ph*), 3.99 – 3.91 (m, 1H, *CH*), 3.91 – 3.79 (m, 2H, CH_2), 2.57 – 2.47 (m, 1H, *CH*), 2.34 – 2.24 (m, 1H, *CH*), 1.94 – 1.79 (m, 2H, CH_2), 1.76 – 1.63 (m, 3H, *CH,* CH_2); ^{13}C NMR (101 MHz, $CDCl_3$) δ 170.08, 136.13, 129.44, 129.15, 126.62, 124.11, 115.76, 72.56, 63.43, 40.82, 40.36, 27.67, 25.72, 23.44.

3,4,5,5a-tetrahydro-2H-5,11b-methanooxepino[3,2-c]quinolin-6(7H)-one (2b, crossed-product). The crude product was purified by flash chromatography (1:2 ethyl acetate:cyclohexane) to give the product as a colourless solid (24 mg, 24%). EI-MS m/z = 230 $[M + H]^+$. ^{1}H NMR (400 MHz, $CDCl_3$) δ 7.95 (s, 1H, *NH*), 7.43 (dd, J = 7.8, 1.6 Hz, 1H, *Ph*), 7.18 (td, J = 7.6, 1.5 Hz, 1H, *Ph*), 7.04 (td, J = 7.6, 1.2 Hz, 1H, *Ph*), 6.70 (dd, J = 7.9, 1.2 Hz, 1H, *Ph*), 4.20 – 4.14 (m, 2H, CH_2), 3.26 – 3.19 (m, 1H, *CH*), 3.07 – 2.97 (m, 1H, *CH*), 2.61 (dd, J = 13.4, 8.4 Hz, 1H, *CH*), 2.32 (dd, J = 13.4, 1.5 Hz, 1H, *CH*), 2.15 – 1.98 (m, 3H*, CH,* CH_2), 1.81 – 1.69 (m, 1H, *CH*); ^{13}C NMR (101 MHz, $CDCl_3$) δ 172.73, 134.81, 128.77, 126.79, 125.00, 123.95, 115.17, 79.96, 65.62, 48.87, 39.33, 36.95, 29.84, 29.17.

4,4-dimethyl-3,3a,4,4a-tetrahydro-2H-furo[2',3':2,3]cyclobuta[1,2-c]quinolin-5(6H)-one (3a). The crude product was purified by flash chromatography (1:1 ethyl acetate:cyclohexane) to give the product as a colourless solid (93 mg, 93%). EI-MS m/z = 244 $[M + H]^+$. ^{1}H NMR (400 MHz, $CDCl_3$) δ 8.93 (s, 1H *NH*), 7.29 (dd, J = 7.7, 1.7 Hz, 1H, *Ph*), 7.21 (td, J = 7.7, 1.5 Hz, 1H, *Ph*), 7.04 (td, J = 7.5, 1.2 Hz, 1H, *Ph*), 6.78 (dd, J = 8.0, 1.2 Hz, 1H, *Ph*), 4.42 – 4.33 (m, 1H, *CH*), 4.04 (q, 1H, *CH*), 3.02 (d, J = 1.3 Hz, 1H, *CH*), 2.57 (dd, J = 6.9, 2.5 Hz, 1H, *CH*), 2.16 – 2.00 (m, 2H, CH_2), 1.22 (s, 3H, CH_3), 1.12 (s, 3H, CH_3); ^{13}C NMR (101 MHz, $CDCl_3$) δ 169.39, 136.54, 129.43, 127.50, 124.10, 123.94, 115.91, 79.38, 68.86, 58.17, 51.79, 34.84, 27.80, 26.10, 24.81.

3,3a-dihydro-2H-3,9b-methanofuro[3,2-c]quinolin-4(5H)-one (4a). The crude product was purified by flash chromatography (1:1 ethyl acetate:cyclohexane) to give the product as a colourless solid (92 mg, 92%). EI-MS m/z = 202 $[M + H]^+$. ^{1}H NMR (400 MHz, $CDCl_3$) δ 8.66 (s, 1H, *NH*), 7.43 (dd, J = 7.5, 1.5 Hz, 1H, *Ph*), 7.25 (td, J = 7.7, 1.5 Hz, 1H, *Ph*), 7.10 (td, J = 7.5, 1.1 Hz, 1H, *Ph*), 6.88 (dd, J = 7.9, 1.5 Hz, 1H, *Ph*), 4.15 (d, J = 6.4 Hz, 1H, *CH*), 4.12 (d, J = 6.3 Hz, 1H, *CH*), 3.46 (d, J = 2.9 Hz, 1H, *CH*), 2.78 (d, J = 9.7 Hz, 1H, *CH*), 2.64 (dd, J = 8.4, 3.0 Hz, 1H, *CH*), 1.69 (dd, J = 9.7, 8.4 Hz, 1H, *CH*); ^{13}C NMR (101 MHz, $CDCl_3$) δ 171.09, 137.03, 129.13, 124.01, 123.86, 121.86, 115.59, 86.81, 72.05, 52.77, 42.42, 40.90.

4a-methyl-3,3a,4,4a-tetrahydro-2H-furo[2',3':2,3]cyclobuta[1,2-c]quinolin-5(6H)-one (5a). The crude product was purified by flash chromatography (1:2 ethyl acetate:cyclohexane) to give the product as a colourless solid (17 mg, 43%). EI-MS *m/z* = 230 $[M + H]^+$. ^{1}H NMR (800 MHz, $CDCl_3$) δ 8.97 (s, 1H, *NH*), 7.29 (d, *J* = 7.6 Hz, 1H, *Ph*), 7.19 (t, *J* = 7.3 Hz, 1H, *Ph*), 7.00 (t, *J* = 7.4 Hz, 1H, *Ph*), 6.77 (d, *J* = 7.7 Hz, 1H, *Ph*), 4.55 (t, *J* = 8.4 Hz, 1H, *CH*), 4.25 – 4.20 (m, 1H, *CH*), 3.02 – 2.99 (m, 1H, *CH*), 2.78 – 2.73 (m, 1H, *CH*), 2.00 – 1.93 (m, 1H, *CH*), 1.89 – 1.84 (m, 1H, *CH*), 1.77 (dd, *J* = 12.9, 5.5 Hz, 1H, *CH*), 1.41 (s, 3H, CH_3). ^{13}C NMR (201 MHz, $CDCl_3$) δ 178.81, 135.12, 128.81, 125.57, 124.90, 123.73, 115.31, 87.08, 70.42, 48.07, 43.75, 35.84, 30.39, 17.86.

1,2,3,3a,4,4a-hexahydrocyclopenta[2,3]cyclobuta[1,2-c]quinolin-5(6H)-one (6a). The crude product was purified by flash chromatography (1:1 ethyl acetate:cyclohexane) to give the product as a colourless solid (96 mg, 96%). EI-MS *m/z* = 214 $[M + H]^+$. ^{1}H NMR (400 MHz, $CDCl_3$) δ 9.20 (s, 1H, *NH*), 7.11 (d, *J* = 7.7 Hz, 2H, *Ph*), 7.00 (t, *J* = 7.5 Hz, 1H, *Ph*), 6.78 (d, *J* = 7.6 Hz, 1H, *Ph*), 3.01 (t, *J* = 9.5 Hz, 1H, *CH*), 2.72 – 2.51 (m, 2H, CH_2), 2.19 – 2.03 (m, 3H, *CH,* CH_2), 1.99 – 1.76 (m, 3H, *CH,* CH_2), 1.72 – 1.63 (m, 1H,*CH*); ^{13}C NMR (101 MHz, $CDCl_3$) δ 172.67, 136.31, 127.86, 127.53, 126.24, 123.90, 115.97, 49.76, 48.17, 41.80, 39.96, 33.69, 29.82, 25.96.

2,3,4,4a,5,5a-hexahydro-1H-benzo[2,3]cyclobuta[1,2-c]quinolin-6(7H)-one (7a). The crude product was purified by flash chromatography (1:1 ethyl acetate:cyclohexane) to give the product as a colourless solid (96 mg, 96%). EI-MS *m/z* = 228 $[M + H]^+$. ^{1}H NMR (400 MHz, $CDCl_3$) δ 9.35 (s, 1H, *NH*), 7.26 (d, *J* = 7.9 Hz, 1H, *Ph*), 7.14 (t, *J* = 7.6 Hz, 1H, *Ph*), 7.04 (t, *J* = 7.5 Hz, 1H, *Ph*), 6.81 (d, *J* = 8.0 Hz, 1H, *Ph*), 3.30 (t, *J* = 8.4 Hz, 1H, *CH*), 2.48 – 2.30 (m, 2H, CH_2), 2.00 (q, *J* = 10.1 Hz, 2H, CH_2), 1.89 – 1.20 (m, 7H, CH_2, CH_2, CH_2, *CH*); ^{13}C NMR (101 MHz, $CDCl_3$) δ 172.35, 136.12, 131.54, 127.98, 127.46, 123.86, 115.86, 42.80, 41.05, 39.70, 35.99, 29.98, 29.38, 22.74, 22.60.

4,4-dimethyl-1,2,3,3a,4,4a-hexahydrocyclopenta[2,3]cyclobuta[1,2-c]quinolin-5(6H)-one (8a). The crude product was purified by flash chromatography (1:1 ethyl acetate:cyclohexane) to give the product as a colourless solid (92 mg, 92%). EI-MS *m/z* = 242 $[M + H]^+$. ^{1}H NMR (400 MHz, $CDCl_3$) δ 8.63 (s, 1H, *NH*), 7.14 (d, *J* = 7.7 Hz, 1H, *Ph*), 7.11 (t, *J* = 6.8 Hz, 1H, *Ph*), 7.00 (t, *J* = 7.5 Hz, 1H, *Ph*), 6.72 (d, *J* = 7.8 Hz, 1H, *Ph*), 2.68 (s, 1H, *CH*), 2.31 (d, *J* = 8.3 Hz, 1H, *CH*), 2.08 – 1.86 (m, 4H, CH_2, CH_2), 1.85 – 1.65 (m, 2H, CH_2), 1.10 (s, 6H, CH_3, CH_3); ^{13}C NMR (101 MHz, $CDCl_3$) δ 170.0, 136.36, 129.35, 127.29, 126.95, 123.82, 115.77, 59.36, 50.46, 46.08, 41.78, 38.79, 28.61, 27.03, 26.56, 24.38.

3a-methyl-1,2,3,3a,4,4a-hexahydrocyclopenta[2,3]cyclobuta[1,2-c]quinolin-5(6H)-one (9a). The crude product was purified by flash chromatography (1:1 ethyl acetate:cyclohexane) to give the product as a colourless solid (91 mg, 91%). EI-MS *m/z* = 228 $[M + H]^+$. ^{1}H NMR (400 MHz, $CDCl_3$) δ 8.78 (s, 1H, *NH*), 7.13 (ddd, *J* = 8.3, 5.5, 3.0 Hz, 1H, *Ph*), 7.04 – 6.95 (m, 2H, *Ph*), 6.76 (d, *J* = 7.9 Hz, 1H, *Ph*), 2.93 (dd, *J* = 11.2, 6.9 Hz, 1H, *CH*), 2.37 (t, *J* = 11.8 Hz, 1H, *CH*), 2.14 – 1.90 (m, 5H, CH_2, CH_2, *CH*), 1.71 (dd, *J* = 13.0, 4.5 Hz, 1H, *CH*), 1.54 – 1.43 (m, 1H, *CH*), 0.81 (s, 3H, CH_3); ^{13}C NMR (101 MHz, $CDCl_3$) δ 175.05, 137.11, 127.60, 127.56, 124.39, 123.24, 115.93, 51.77, 49.85, 41.77, 41.61, 38.28, 37.73, 24.85, 24.55.

3,3a,4,4a-tetrahydro-1H-furo[3',4':2,3]cyclobuta[1,2-c]quinolin-5(6H)-one (10a). The crude product was purified by flash chromatography (1:1 ethyl acetate:cyclohexane) to give the product as a colourless solid (97 mg, 97%). EI-MS *m/z* = 216 $[M + H]^+$. ^{1}H NMR (400 MHz, $CDCl_3$) δ 8.96 (s, 1H, *NH*), 7.22 – 7.14 (m, 2H, *Ph*), 7.03 (td, *J* = 7.4, 1.2 Hz, 1H, *Ph*), 6.81 (d, *J* = 8.3 Hz, 1H, *Ph*), 4.09 (d, *J* = 9.5 Hz, 1H, *CH*), 4.02 (d, *J* = 9.7 Hz, 1H, *CH*), 3.94 (dd, *J* = 9.6, 5.6 Hz, 1H, *CH*), 3.79 (d, *J* = 9.6 Hz, 1H, *CH*), 3.30 (dd, *J* = 10.8, 8.0 Hz, 1H, *CH*), 2.90 (dd, *J* = 8.9, 4.7 Hz, 1H, *CH*), 2.60 (dt, *J* = 12.6, 8.6 Hz, 1H, *CH*), 2.31 (ddd, *J* = 12.6, 10.8, 4.0 Hz, 1H, *CH*); ^{13}C NMR (101 MHz, $CDCl_3$) δ 171.64, 137.10, 128.48, 126.30, 123.95, 122.53, 116.30, 79.54, 75.32, 50.80, 49.19, 39.53, 29.38.

3a-methyl-3,3a,4,4a-tetrahydro-1H-furo[3',4':2,3]cyclobuta[1,2-c]quinolin-5(6H)-one (11a). The crude product was purified by flash chromatography (1:1 ethyl acetate:cyclohexane) to give the product

as a colourless solid (89 mg, 89%). EI-MS *m/z* = 230 $[M + H]^+$. ^{1}H NMR (400 MHz, $CDCl_3$) δ 8.92 (s, 1H, *NH*), 7.19 (ddd, *J* = 8.4, 5.9, 2.9 Hz, 1H, *Ph*), 7.07 – 6.99 (m, 2H, *Ph*), 6.83 (d, *J* = 7.9 Hz, 1H, *Ph*), 4.14 (d, *J* = 9.6 Hz, 1H, *CH*), 3.97 (d, *J* = 9.3 Hz, 1H, *CH*), 3.88 (d, *J* = 9.7 Hz, 1H, *CH*), 3.48 (d, *J* = 9.3 Hz, 1H, *CH*), 3.22 (dd, *J* = 11.0, 7.2 Hz, 1H, *CH*), 2.60 (t, *J* = 11.7 Hz, 1H, *CH*), 2.16 (dd, *J* = 12.4, 7.2 Hz, 1H, *CH*), 0.88 (s, 3H, CH_3); ^{13}C NMR (101 MHz, $CDCl_3$) δ 171.96, 137.83, 128.55, 127.42, 123.45, 119.37, 116.41, 81.13, 79.80, 52.89, 51.11, 37.72, 37.09, 19.96.

4,4-dimethyl-3,3a,4,4a-tetrahydro-1H-furo[3',4':2,3]cyclobuta[1,2-c]quinolin-5(6H)-one (12a). The crude product was purified by flash chromatography (1:1 ethyl acetate:cyclohexane) to give the product as a colourless solid (95 mg, 95%). EI-MS *m/z* = 244 $[M + H]^+$. ^{1}H NMR (400 MHz, $CDCl_3$) δ 8.62 (s, 1H, *NH*), 7.23 – 7.12 (m, 2H, *Ph*), 7.02 (t, *J* = 7.5 Hz, 1H, *Ph*), 6.76 (d, *J* = 7.9 Hz, 1H, *Ph*), 4.23 (d, *J* = 10.3 Hz, 1H, *CH*), 3.99 (d, *J* = 9.4 Hz, 1H, *CH*), 3.82 (dd, *J* = 10.3, 6.1 Hz, 1H, *CH*), 3.58 (d, *J* = 9.3 Hz, 1H, *CH*), 2.90 (s, 1H, *CH*), 2.51 (d, *J* = 6.0 Hz, 1H, *CH*), 1.20 (s, 3H, CH_3), 1.16 (s, 3H, CH_3); ^{13}C NMR (101 MHz, $CDCl_3$) δ 169.03, 137.19, 128.26, 126.82, 123.82, 123.44, 116.15, 78.79, 70.48, 60.29, 50.47, 46.47, 38.46, 25.81, 24.46.

6-methyl-3,3a,4,4a-tetrahydro-2H-furo[2',3':2,3]cyclobuta[1,2-c]quinolin-5(6H)-one (13a, straight-product). The crude product was purified by flash chromatography (1:3 ethyl acetate:cyclohexane) to give the product as a colourless solid (79 mg, 79%). EI-MS *m/z* = 229 $[M + H]^+$. ^{1}H NMR (400 MHz, $CDCl_3$) δ 7.37 – 7.29 (m, 2H, *Ph*), 7.09 (td, *J* = 7.5, 1.1 Hz, 1H, *Ph*), 7.01 (dd, *J* = 8.3, 1.1 Hz, 1H, *Ph*), 4.44 (ddd, *J* = 9.4, 7.9, 1.5 Hz, 1H, *CH*), 4.22 (ddd, *J* = 11.1, 9.2, 5.7 Hz, 1H, *CH*), 3.39 (s, 4H, *CH,* CH_3^*), 2.91 (td, *J* = 8.5, 5.5 Hz, 1H, *CH*), 2.33 (ddd, *J* = 12.9, 9.0, 6.7 Hz, 1H, *CH*), 2.26 – 2.06 (m, 2H, CH_2), 1.83 (ddt, *J* = 12.8, 5.7, 1.4 Hz, 1H, *CH*). ^{13}C NMR (101 MHz, $CDCl_3$) δ 170.42, 139.06, 129.43, 126.73, 125.26, 123.55, 114.59, 82.19, 68.67, 46.48, 42.35, 32.43, 29.34, 27.23. *Methyl and aliphatic CH peaks overlap.

6-methyl-2,3,4,4a-tetrahydro-4,10b-methanopyrano[3,2-c]quinolin-5(6H)-one (13b, crossed-product). The crude product was purified by flash chromatography (1:3 ethyl acetate:cyclohexane) to give the product as a colourless solid (18 mg, 18%). EI-MS *m/z* = 229 $[M + H]^+$. ^{1}H NMR (400 MHz, $CDCl_3$) δ 7.44 (dd, *J* = 7.5, 1.6 Hz, 1H, *Ph*), 7.32 – 7.26 (m, 1H, *Ph*), 7.10 (td, *J* = 7.5, 1.1 Hz, 1H, *Ph*), 7.00 (dd, *J* = 8.2, 1.1 Hz, 1H, *Ph*), 4.39 (dt, *J* = 11.3, 7.6 Hz, 1H, *CH*), 4.25 (ddd, *J* = 11.6, 7.9, 4.1 Hz, 1H, *CH*), 3.43 (s, 3H, CH_3), 3.08 (ddd, *J* = 6.1, 4.1, 2.4 Hz, 1H, *CH*), 2.86 (d, *J* = 8.0 Hz, 1H, *CH*), 2.50 (ddd, *J* = 10.9, 5.8, 1.6 Hz, 1H, *CH*), 2.45 – 2.30 (m, 1H, *CH*), 2.29 – 2.20 (m, 1H, *CH*), 2.15 (dd, *J* = 10.9, 8.0 Hz, 1H, *CH*). ^{13}C NMR (101 MHz, $CDCl_3$) δ 171.35, 138.49, 128.78, 126.90, 123.95, 123.50, 114.67, 78.95, 60.92, 50.82, 37.47, 36.28, 31.58, 29.76.

1-acetyl-2,2a,4,8b-tetrahydrocyclobuta[c]quinolin-3(1H)-one (14). The crude product was purified by flash chromatography (1:2 ethyl acetate:cyclohexane) to give the product as a colourless solid (83 mg, 56%). EI-MS *m/z* = 216 $[M+H]^+$. ^{1}H NMR (400 MHz, $CDCl_3$) δ 8.86 (s, 1H, *NH*), 7.19 (td, *J* = 7.7, 1.5 Hz, 1H, *Ph*), 7.11 (d, *J* = 7.4 Hz, 1H, *Ph*), 7.00 (t, *J* = 7.5 Hz, 1H, *Ph*), 6.81 (d, *J* = 7.9 Hz, 1H, *Ph*), 3.98 (t, *J* = 8.8 Hz, 1H, *CH*), 3.47 (q, *J* = 9.0 Hz, 1H, *CH*), 3.24 (td, *J* = 9.5, 3.1 Hz, 1H, *CH*), 2.79 (dt, *J* = 11.9, 9.7 Hz, 1H, *CH*), 2.60 (ddd, *J* = 12.0, 9.0, 3.1 Hz, 1H, *CH*), 2.11 (s, 3H, CH_3). ^{13}C NMR (101 MHz, $CDCl_3$) δ 207.07, 172.72, 136.88, 128.51, 128.03, 123.93, 122.89, 115.94, 52.79, 39.15, 34.32, 28.87, 28.16.

1-propionyl-2,2a,4,8b-tetrahydrocyclobuta[c]quinolin-3(1H)-one (15). The crude product was purified by flash chromatography (1:2 ethyl acetate:cyclohexane) to give the product as a colourless solid (91 mg, 58%). EI-MS *m/z* = 230 $[M+H]^+$. ^{1}H NMR (800 MHz, $CDCl_3$) δ 8.93 (s, 1H, *NH*), 7.18 (td, *J* = 7.6, 1.4 Hz, 1H, *Ph*), 7.08 (dd, *J* = 7.5, 1.4 Hz, 1H, *Ph*), 6.99 (td, *J* = 7.5, 0.8 Hz, 1H, *Ph*), 6.81 (d, *J* = 7.9 Hz, 1H, *Ph*), 4.00 (t, *J* = 8.8 Hz, 1H, *CH*), 3.48 (q, *J* = 9.0 Hz, 1H, *CH*), 3.27 – 3.22 (m, 1H, *CH*), 2.78 (dt, *J* = 11.8, 9.7 Hz, 1H, *CH*), 2.60 (ddd, *J* = 12.0, 8.9, 2.9 Hz, 1H, *CH*), 2.42 – 2.30 (m, 2H, CH_2), 1.06 (t, *J* = 7.3 Hz, 3H, CH_3). ^{13}C NMR (201 MHz, $CDCl_3$) δ 209.88, 172.92, 136.87, 128.46, 127.98, 123.91, 122.99, 115.95, 51.77, 39.15, 34.53, 34.34, 29.12, 7.65.

Preparation of chiral standards:

The enantiomers of **1a** were separated by preparative chiral UPLC by Reach Separations (Nottingham) to afford (-)-**1a** (98.2% e.e.) and (+)-**1a** (99.6% e.e.) as white solids. The absolute stereochemistry was determined by measuring the optical rotation (-)-**1a** (−72.0°) (+)-**1a** (+72.0°) at 0.017 g ml^{-1} in methanol (MeOH) at 26 °C.

Crystallization, refinement and model building:

EnT1.0 and EnT1.3 were crystallised by mixing 200 nl of 15 mg ml^{-1} protein in 20mM HEPES buffer, pH 7.5) with equal volumes of precipitant. All trials were conducted by sitting-drop vapour diffusion and incubated at 20 °C. Crystals of EnT1.3$\Delta C_{310\text{-}314}$ (expressed with an N-terminal His_6-tag with 310-314 and the protein-tag linker deleted) co-crystallised with optically pure product (-)-**1a** were obtained by incubating 0.25mg ml^{-1} protein with 0.75mg ml^{-1} of (-)-**1a** in buffer (20mM HEPES, pH 7.5) at room temperature on a roller shaker for 18 hr. The sample was concentrated to ~10mg ml^{-1} and trays were laid using the sitting-drop vapour diffusion method by mixing 200 nl of protein with equal volumes of precipitant and incubating at 20 °C. Crystallisation conditions were identified using the PACT and JCSG-plus screens (Molecular Dimensions) and are provided in Supplementary Information, Table S4.

Prior to data collection crystals were cryo-protected by the addition of 20% PEG 200 to the mother liquor and plunge cooled in liquid nitrogen. All data were collected at Diamond Light Source (Harwell, UK) using beamline i03. Data reduction was performed with Dials and the structure solved by molecular replacement using a search model derived from the structure of DA20_00_00_A74I (PDB: 3I1C). Iterative rounds of model building and refinement were performed in COOT and Phenix.refine, respectively.[40] Validation with MOLPROBITY and PDBREDO[41] were incorporated into the iterative rebuild and refinement process. Data collection and refinement statistics are shown in Supplementary Information, Table S5. The coordinates and structure factors for EnT1.0, EnT1.3, and a EnT1.3$\Delta C_{310\text{-}314}$ with bound product (-)-**1a** have been deposited in the Protein Data Bank under accession numbers 7ZP5, 7ZP6 and 7ZP7, respectively. Residual F_O-F_C density is observed near the active site in the structure of EnT1.0 that could not readily be modelled by any components of the crystallisation mix.

Methods References

40. Adams s, P. D. et al. PHENIX: a comprehensive Python-based system for macromolecular structure solution. *Acta Crystallogr. D* **66**, 213–221 (2010).

41. Joosten, R. P., Joosten, K., Cohen, S. X., Vriend, G. & Perrakis, A. Automatic rebuilding and optimization of crystallographic structures in the Protein Data Bank. Bioinformatics 27, 3392–3398 (2011).

Extended Data Figures:

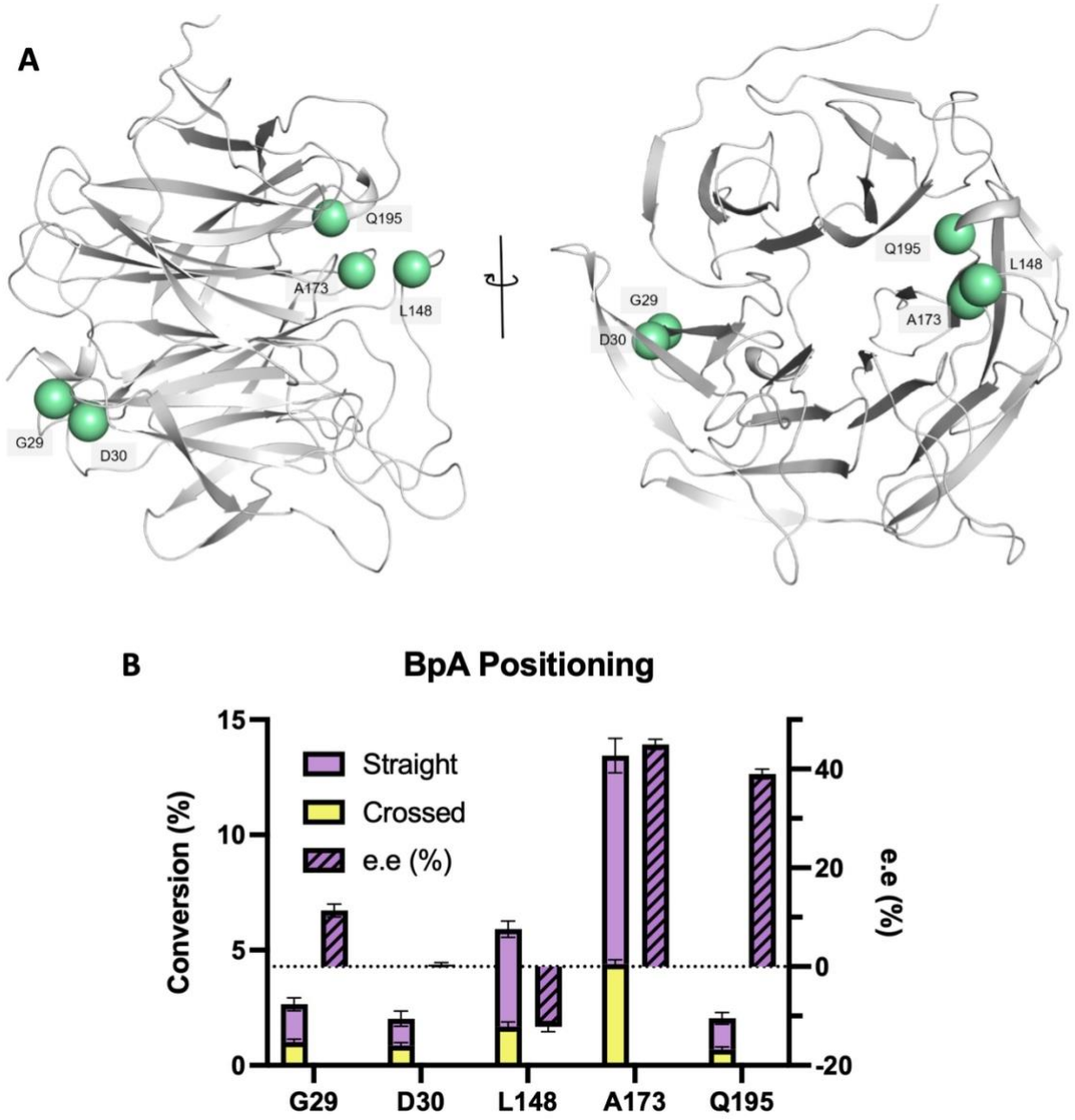

Extended Data Figure 1: BpA positioning in the DA_20_00 scaffold. A) Positions within DA_20_00 selected to incorporate the photosensitiser 4-benzoylphenylalanine (BpA) are shown as green CPK spheres at the C-alpha. B) Bar chart showing reaction conversions and selectivities achieved by DA_20_00 variants with BpA installed at the specified positions. Reaction conditions: 15 μM catalyst, 400 μM **1**, 30 minutes irradiation (10 seconds on/off pulse) at 365 nm, 4 °C, 100 μL PBS (pH 7.4) with 5% DMSO as a cosolvent in a 96-well plate. Enantiomeric excess is given for the major product, (-)-**1a**. Error bars represent the standard deviation of measurements made in triplicate.

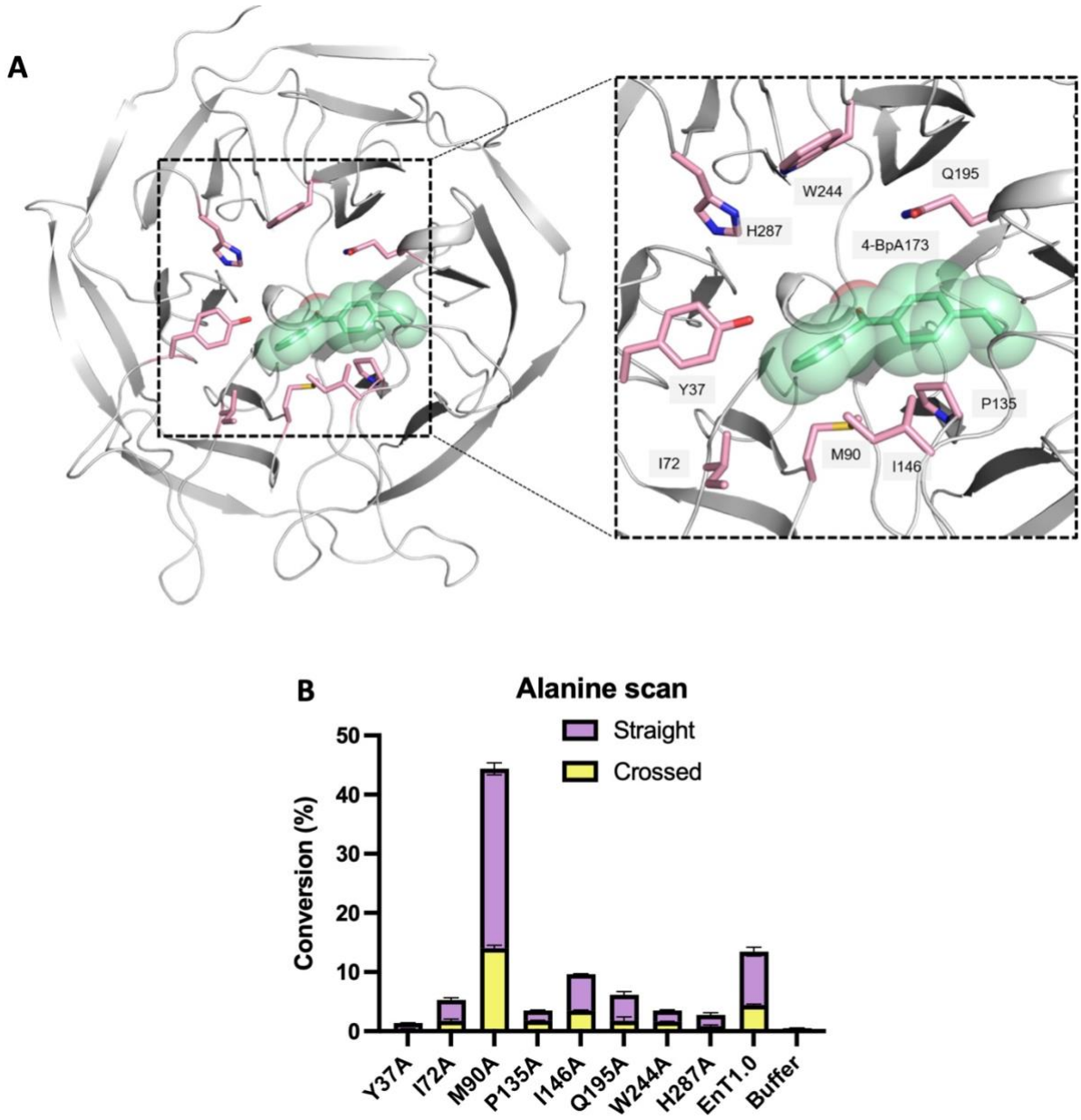

Extended Data Figure 2: Summary of alanine scan of EnT1.0 A) Positions within EnT1.0 selected for the alanine scan of the active site are shown as atom-coloured sticks with pink carbon atoms. BpA173 is shown in green CPK spheres. B) Bar chart showing reaction conversions and regioselectivities achieved by EnT1.0 variants. Reaction conditions: 15 μM catalyst, 400 μM **1**, 30 minutes irradiation (10 seconds on/off pulse) at 365 nm, 4 °C, 100 μL PBS (pH 7.4) with 5% DMSO as a cosolvent in a 96-well plate. Error bars represent the standard deviation of measurements made in triplicate.

Round	Substrate	Description	Clones Screened	Beneficial Mutations	Best Variant
Alanine Scan	**1**	**Alanine scan** of active site: Y37, I72, M90, P135, I146, Q195, W244, H287	8	M90A	EnT1.1= EnT1.0 + M90A
1	**1**	**Saturation mutagenesis** of active site positions: A74, M90, A120, Y121, P135, I146, L148, Q149, A175, Q195, K225, A229, E268, K269, S271, W244, H287	1,496	Q149D, K225V, A229S	EnT1.2= EnT1.1 + Q149D_A229S
2	**1**	**Saturation mutagenesis** of active site positions: G19, A21, Y37, I72, Y121, T133, A136, F144, S147, G153, Q172, P174, G176, Q195, P196, K225, G226, G227, A242, W244, S271, A272	1,936	Y37L, P196R, K225E, W244M	EnT1.3= EnT1.2 + P196R_K225E
3	**13**	**Saturation mutagenesis** of active site positions (template EnT1.3 + Y121F): A21, V34, P36, Y37, I72, A74, A120, Y121, T133, F144, I146, L148, A175, A193, H224, S229, W244, K269, S271, H287	1,760	Y37G, Y37L, Y37W, I74V, F121A, F121N, A210G, S271 A, S271C	EnT1.3 Y121F S271C

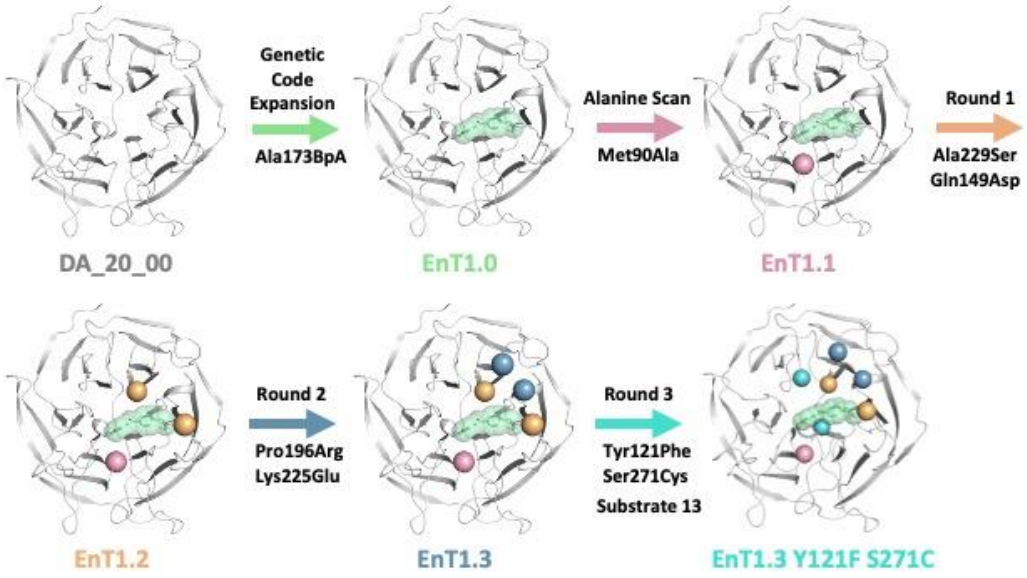

Extended Data Figure 3: Directed evolution of an efficient and enantioselective photoenzyme. Schematic showing the trajectory from DA_20_00 to EnT1.3 and EnT1.3 Y121F S271C. Mutations introduced are represented as CPK spheres at the C-alpha. The original design DA_20_00 contains 13 mutations built into a 6-bladed β-propeller scaffold (PDB 1E1A; a diisopropylfluorophosphatase from *Loligo Vulgaris)*.[13] Incorporation of the photosensitiser BpA (green atom-coloured sticks and semi-transparent CPK spheres) at position A173 provided EnT1.0. An alanine scan of EnT1.0 highlighted one variant with increased activity, providing EnT1.1. Two rounds of evolution afforded EnT1.3, which contains six mutations when compared to the original design DA_20_00. EnT1.3 was further evolved towards substrate 13 resulting in EnT1.3 Y121F S271C. Library generation method, positions targeted,

the number of clones evaluated, beneficial mutations and the most improved variant for each round are given in the table.

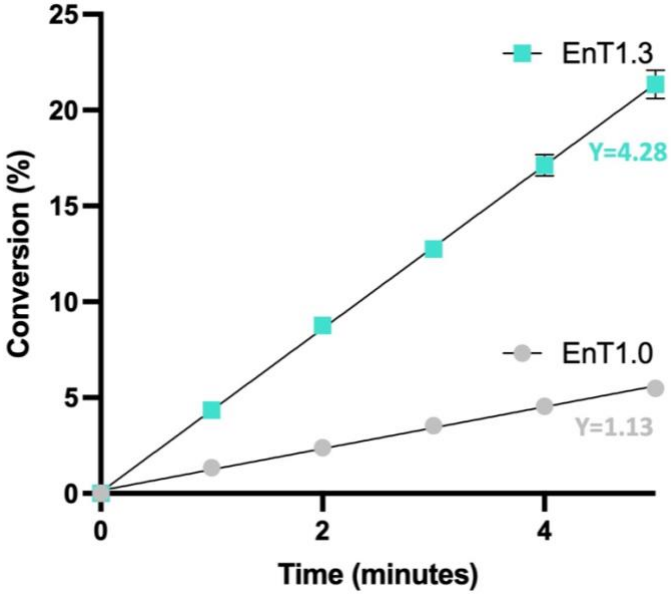

Extended Data Figure 4: Reaction time-courses of EnT1.0 and EnT1.3. Reaction conditions: 15 μM catalyst, 400 μM **1**, 10 seconds on/off pulse at 365 nm, 4 °C, 1 mL PBS (pH 7.4) with 5% DMSO as a cosolvent in 2 mL glass vials. At each time point, 100 μL of reaction mix was quenched with 1 volume MeCN and analysed by UPLC. Reaction conversion of **1** to **1a** and **1b** is given over 5 minutes. The gradients of a linear fit to the data are given for each variant. A table providing conversion data is given in Supplementary Information Table S2. Error bars represent the standard deviation of measurements made in triplicate (error bars are not shown where they are smaller than the data point marker).

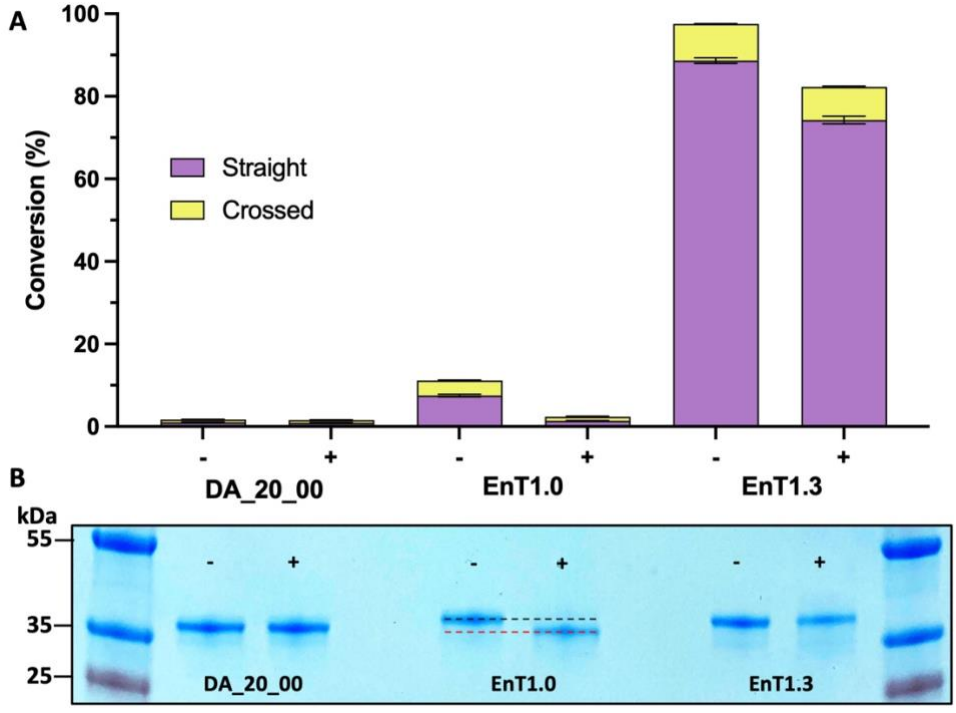

Extended Data Figure 5. Photodamage of EnT1.0 and EnT1.3. To investigate the effects of photodamage, aliquots of 30 μM enzyme in PBS (pH 7.4) were pre-irradiated for 90 minutes (10 seconds on/off pulse at 365 nm) at 4 °C, before performing reactions. Control aliquots of enzyme were incubated in the dark at 4 °C. A) Bar chart displaying the conversion of **1** to **1a** and **1b** achieved by variants DA_20_00, EnT1.0 and EnT1.3 that had been pre- irradiated with light (+) and had been incubated in the dark (-). Reaction conditions: 15 μM catalyst, 400 μM **1**, 30 minutes irradiation (10 seconds on/off pulse) at 365 nm, 4 °C, PBS (pH 7.4) with 5% DMSO as a cosolvent. Error bars represent the standard deviation of measurements made in triplicate. B) SDS-PAGE analysis of protein variants (DA_20_00, EnT1.0, EnT1.3.) that had been pre-irradiated with light (+) and had been incubated in the dark (-).

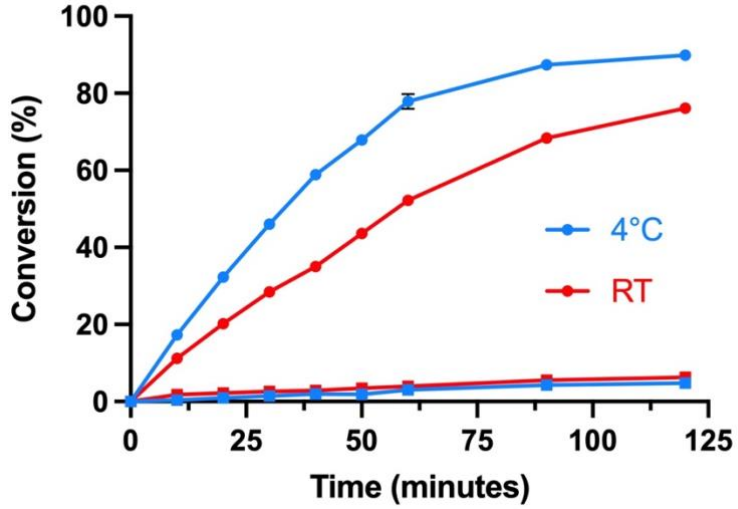

Extended Data Figure 6: Temperature dependence of EnT1.3. Reaction conditions: 2.25 μM catalyst (7.5 mol%), 300 μM **1**, 10 seconds on/off pulse at 365 nm, in PBS (pH 7.4) with 5% DMSO as a cosolvent at a specified temperature. A time course providing the conversion of **1** to **1a** and **1b** at 4 °C (blue circles) and room temperature (red circles). A negative control containing no catalyst is shown at 4 °C and room temperature (blue squares and red squares, respectively). Error bars represent the standard deviation of measurements made in triplicate.

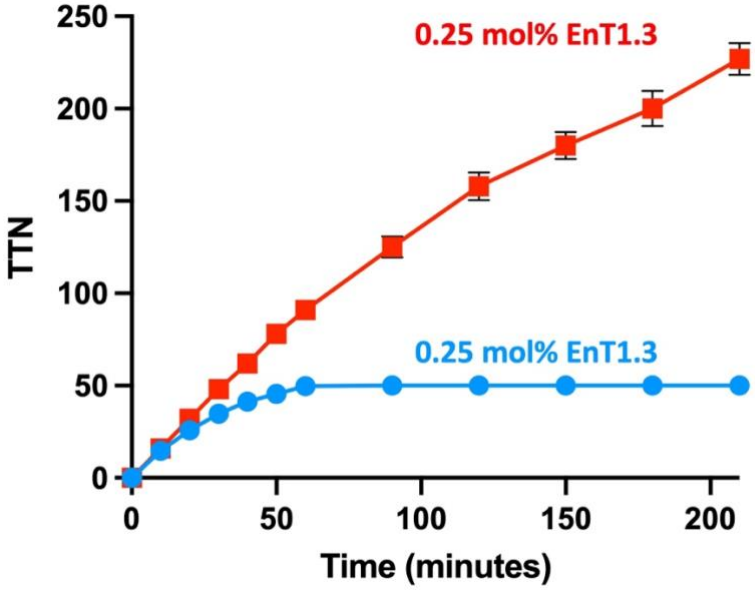

Extended Data Figure 7: Total turnover numbers achieved by EnT1.3. Reaction conditions: 800 μM **1**, 10 seconds on/off pulse at 365 nm, at 4 °C, in 1 mL PBS (pH 7.4) with 10% DMSO as a cosolvent, at a specified catalyst loading. A time course providing the reaction conversion of **1** to **1a** and **1b** at 0.2 mol% and 1.5 mol% catalyst loading (1.6 μM, red and 12 μM, blue, respectively). A background correction has been applied to both curves, corresponding to less than 10% of turnovers. Error bars represent the standard deviation of measurements made in triplicate (error bars are not shown where they are smaller than the data point marker).

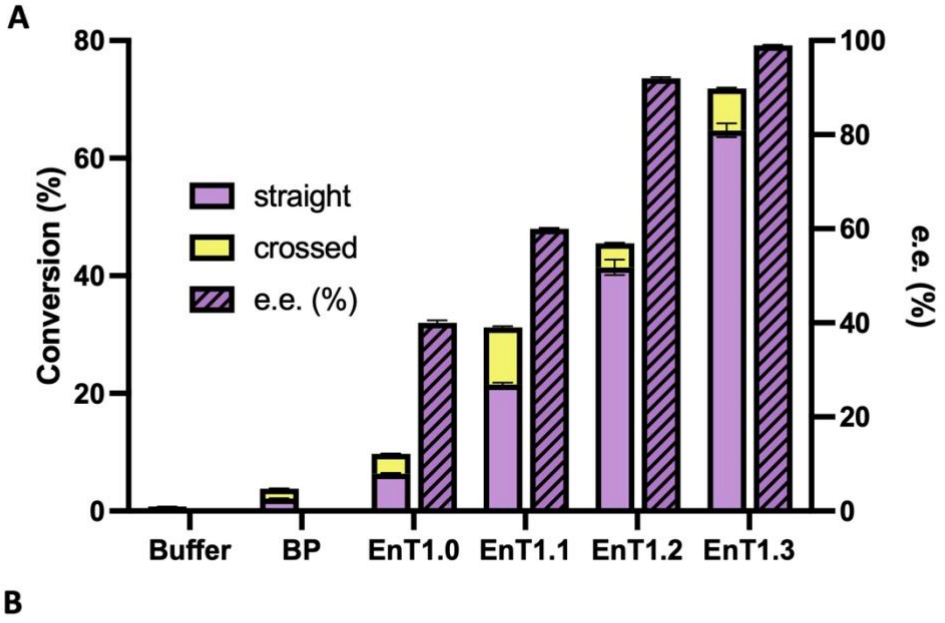

B

	Average straight conversion (%)	S.D.	Average crossed conversion (%)	S.D.	Straight *e.e.* (%)	S.D.
Buffer	0.41	0.03	0.32	0.00	0	-
BP	2.13	0.03	1.70	0.02	0	-
EnT1.0	6.36	0.14	3.35	0.07	40	0.51
EnT1.1	21.51	0.34	9.70	0.20	60	0.17
EnT1.2	41.46	1.32	4.05	0.12	92	0.21
EnT1.3	64.73	1.19	7.13	0.12	99	0.12

Extended Data Figure 8: Evolution trajectory. Reaction conditions: 10 μM catalyst, 400 μM **1**, 30 minutes irradiation (10 seconds on/off pulse) at 365 nm, 4 °C, PBS (pH 7.4) with 5% DMSO as a cosolvent in glass vials. A) Bar chart showing conversion of **1** to **1a** and **1b** and enantiomeric excess for the major product, (-)-**1a** achieved by selected variants along the evolutionary trajectory. Error bars represent the standard deviation of measurements made in triplicate (error bars are not shown where they are smaller than the data point marker). B) Table providing conversion and selectivity data for Extended Data Figure 8A.

A

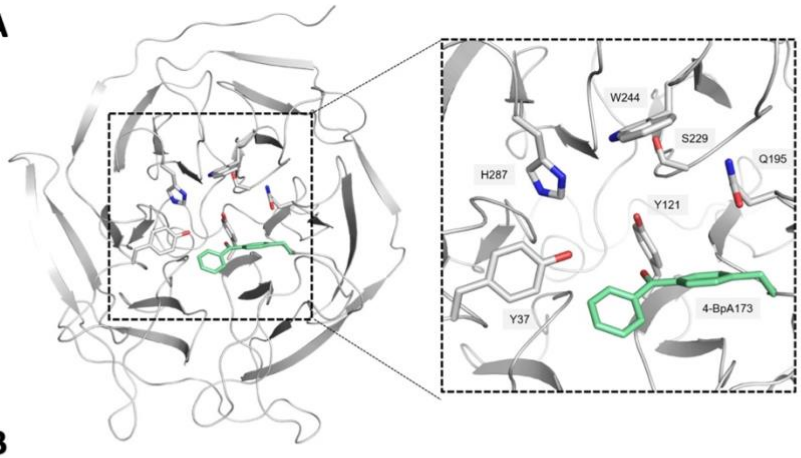

B

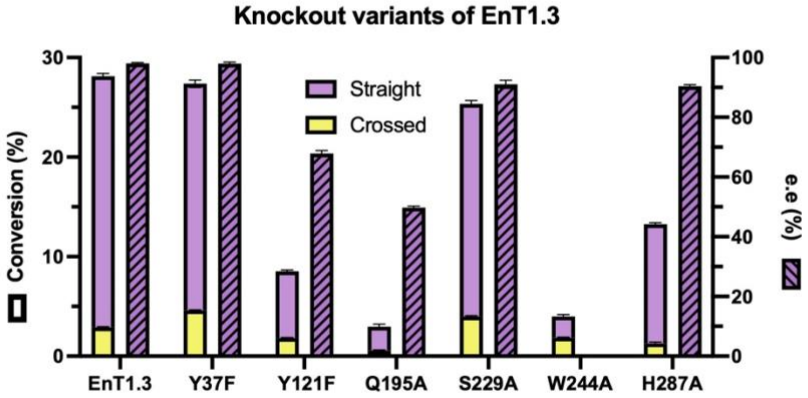

C

Variant	Average Straight Conversion (%)	S.D.	Average Crossed Conversion (%)	S.D.	Straight *e.e.* (%)	S.D.
EnT1.3	24.8	0.810	2.9	0.058	98	0.28
EnT1.3 Y37F	22.5	0.656	4.6	0.115	98	0.52
EnT1.3 Y121F	6.9	0.487	1.8	0.043	67	1.0
EnT1.3 Q195A	2.6	0.604	0.6	0.107	50	0.51
EnT1.3 S229A	21.1	0.585	3.9	0.120	91	1.4
EnT1.3 W244A	2.4	0.537	1.8	0.058	0	0.43
EnT1.3 H287A	12.1	0.211	1.3	0.113	90	0.53

Extended Data Figure 9: Knockout variants of EnT1.3. A) Positions in EnT1.3 selected for a mutational scan are shown as atom-coloured sticks, with carbon grey. BpA is shown as atom-coloured sticks with carbon green. B) Reaction conditions: 7.5 µM catalyst, 400 µM **1**, 15 minutes irradiation (10 seconds on/off pulse) at 365 nm, 4 °C, 100 µL PBS (pH 7.4) with 5% DMSO as a cosolvent in 96-well plates. Bar chart showing conversions and enantiomeric excess for the major product, (-)-**1a**, achieved by EnT1.3 variants. Error bars represent the standard deviation of measurements made in triplicate. C) Table providing conversion and selectivity data for Extended Data Fig 9B.

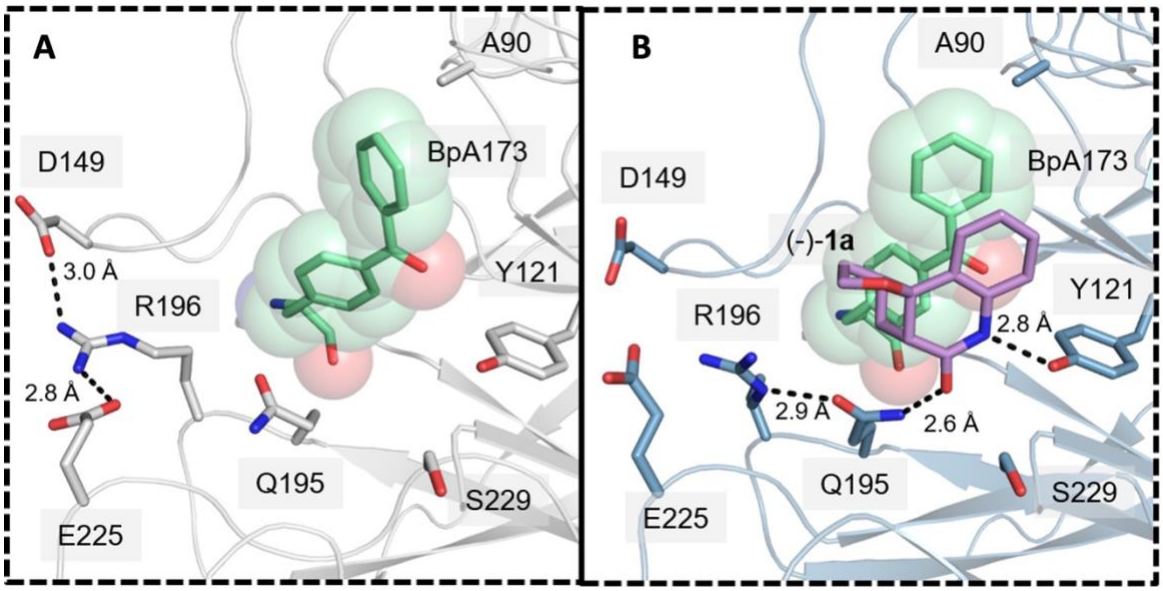

Extended Data Figure 10. Comparison of *apo*-EnT1.3 (PDB: 7ZP6) and product- bound EnT1.3ΔC310-314 (PDB: 7ZP7). A) EnT1.3 (shown as grey cartoon) has a hydrogen bonding network formed of E225, R196, and D149 (shown as black dashed lines). The side chains of key residues are shown as atom-coloured sticks with grey carbons. BpA173 is shown as atom-coloured sticks and semi-transparent CPK spheres with green carbons. B) The structure of EnT1.3ΔC310-314 (shown as a blue cartoon) in complex with the product (-)-**1a** (shown as atom-coloured sticks with purple carbons). The side chains of key residues are shown as atom-coloured sticks with blue carbons. BpA173 is shown as atom-coloured sticks and semi-transparent CPK spheres with green carbons. When in complex with product, R196 lies in a different conformation to that shown in the structure of *apo*-EnT1.3, instead forming a hydrogen bond with Q195. Q195 and Y121 form close hydrogen bonds to (-)-**1a**.